

## Magnetization switching probability in the dynamical switching regime driven by spin-transfer torque


Tomohiro Taniguchi<sup>1</sup>,<sup>2</sup> Shinji Isogami,<sup>2</sup> Yohei Shiokawa,<sup>3</sup> Yugo Ishitani,<sup>3</sup> Eiji Komura,<sup>3</sup> Tomoyuki Sasaki,<sup>3</sup> Seiji Mitani,<sup>2</sup> and Masamitsu Hayashi<sup>2,4</sup>

<sup>1</sup>National Institute of Advanced Industrial Science and Technology (AIST),  
Spintronics Research Center, Tsukuba, Ibaraki 305-8568, Japan

<sup>2</sup>National Institute for Materials Science, Tsukuba 305-0047, Japan

<sup>3</sup>Advanced Products Development Center, Technology & Intellectual Property HQ,  
TDK Corporation, Ichikawa, Chiba 272-8558, Japan

<sup>4</sup>The University of Tokyo, Tokyo 113-8654, Japan

 (Received 27 April 2022; revised 20 July 2022; accepted 12 September 2022; published 28 September 2022)

We study magnetization switching in the dynamical regime for in-plane magnetized systems, useful for field-free spin-orbit torque switching devices. We derive a formula for the switching probability, characterized by the thermal stability factor, critical current density, and the linewidth of ferromagnetic resonance. The formula agrees well with numerical simulations based on the Landau-Lifshitz-Gilbert equation. To study the viability of the theory developed, the switching probability of an in-plane magnetized ferromagnet in three-terminal spin-orbit torque switching devices is measured. We find that the transition width of the switching probability versus current increases with decreasing pulse width. The shape of the probability density, the current derivative of the switching probability, changes with varying pulse width. These characteristics are in good agreement with the theory developed. From the analyses, we show that the dynamical and thermally activated switching regimes can be distinguished simply from the shape of the probability density. The formula therefore provides useful means to analyze the switching probability of two-terminal spin torque and three-terminal spin-orbit torque switching devices.

DOI: [10.1103/PhysRevB.106.104431](https://doi.org/10.1103/PhysRevB.106.104431)

### I. INTRODUCTION

Current-induced magnetization dynamics in nanostructured ferromagnets [1–3] have attracted significant attention from the viewpoints of fundamental and applied physics [4–10]. It has a quantum-mechanical nature in which spin angular momentum of conduction electrons is transferred to the magnetization of the ferromagnet via spin-transfer torque. Current-induced magnetization switching and auto-oscillation can be used for nonvolatile memories, microwave generators, and random-number generators [11–18].

Magnetization dynamics have a stochastic behavior due to thermal fluctuations [19], which, for example, cause a nonzero retention time of magnetization switching and linewidth broadening of auto-oscillation. Magnetization switching at finite temperature is classified into two regimes depending on the applied current density. It is convenient to introduce a threshold current density  $J^*$ , which corresponds to a minimum current density to induce switching at zero temperature with an infinite pulse width. In the thermally activated regime, where current density  $J$  is smaller than  $J^*$ , energy injection from a thermal bath is necessary. The switching probability in the thermally activated regime has been extensively studied [20–30]. When  $J$  is larger than  $J^*$ , the dynamical or precessional switching regime takes place.

The switching process is highly probabilistic in the thermally activated regime, i.e., it depends on the thermal energy

provided by the environment. The average time required to switch the magnetization in this regime is thus significantly longer than that of the dynamical switching regime. Since the industry aims to develop faster switching devices, particularly for memories that make use of spin-orbit torque switching [28,31–35], switching in the dynamical regime is preferred. The analyses of the switching probability in the dynamical switching regime, however, have been mainly limited to perpendicularly magnetized ferromagnets [25,36–38], which is in contrast to the thermally activated regime where analytical formulas have been derived for both perpendicularly and in-plane magnetized ferromagnets [20,39–47]. These facts motivate us to revisit the analysis of the magnetization switching of in-plane magnetized ferromagnets in the dynamical switching regime.

In this work, we show theoretical and experimental analyses of current-induced magnetization switching of in-plane magnetized ferromagnets in the dynamical switching regime. We derive a formula of the switching probability applicable to fast magnetization switching by solving the Landau-Lifshitz-Gilbert (LLG) equation analytically. The formula generalizes the solution obtained for perpendicularly magnetized ferromagnets and has a wide range of applicability. We compare the formula to numerical simulations of the LLG equation and find quantitative agreement between the two. To assess the relevance of the formula, spin-orbit torque induced

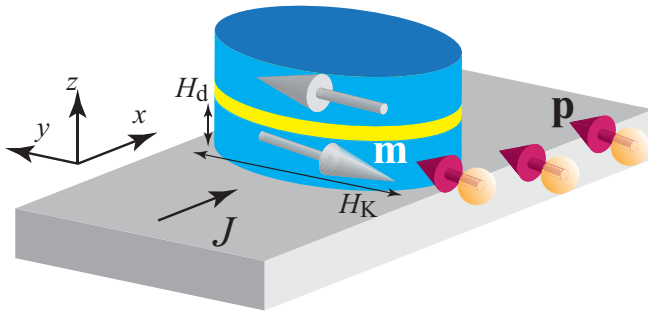


FIG. 1. Schematic illustration of a three-terminal device that consists of a current channel and a MTJ. The magnetic easy axis of the free layer (bottom blue layer) and the reference layer (top blue layer) point along the film plane. The unit vector  $\mathbf{m}$  represents the magnetization direction of the free layer. The current density  $J$  flows in the channel along the  $x$  direction. Due to the spin Hall effect of the channel material, spin current with spin polarization  $\mathbf{p}$  flows into the free layer. The yellow spheres with a red arrow represent the flow of spin current. Definition of the coordinate axis is included. In the system under consideration, the in-plane magnetic anisotropy field  $H_K$  points along the  $y$  axis while the effective demagnetization field  $H_d$  is parallel to the  $z$  axis.

magnetization switching of in-plane magnetized ferromagnets is studied experimentally. The magnetization switching probability is obtained for various current pulse amplitudes and widths. We find that the transition width of the switching probability increases with decreasing pulse width. An asymmetry in the shape of the probability density, i.e., the current density derivative of the switching probability, is identified for shorter current pulses. The degree of asymmetry increases with decreasing pulse width. These results can be accounted for using the formula developed. In particular, we show that the shape of the probability density provides straightforward means to distinguish the dynamical and thermally activated switching regimes.

The paper is organized as follows. In Sec. II, we derive a theoretical formula of the switching probability in the dynamical switching regime, and we compare it with that obtained from numerical simulations. In Sec. III, we compare the theory with experiments conducted using three-terminal spin-orbit torque switching devices. The conclusion of this work is summarized in Sec. IV.

## II. THEORETICAL AND NUMERICAL ANALYSES OF MAGNETIZATION SWITCHING

In this section, we summarize the derivation of the switching probability formula. As described in Sec. I, the present work is motivated to address spin-orbit torque induced magnetization switching in three-terminal devices schematically shown in Fig. 1, where the magnetization in the free layer points along the  $y$  direction. While we use an in-plane magnetized ferromagnet as an example, the formulation developed here can be extended to perpendicularly magnetized systems and has wide applicability, as explained in Sec. II C.

### A. Landau-Lifshitz-Gilbert equation

Here, we introduce the LLG equation. We are interested in the dynamics of a uniform magnetization excited by the spin-transfer torque. Studies beyond such a macrospin limit can be found in, for example, Refs. [48–51]. The unit vector pointing along the magnetization direction of the free layer is defined as  $\mathbf{m}$ . The LLG equation is given as

$$\frac{d\mathbf{m}}{dt} = -\gamma\mathbf{m} \times \mathbf{H} - \gamma H_s \mathbf{m} \times (\mathbf{p} \times \mathbf{m}) + \alpha \mathbf{m} \times \frac{d\mathbf{m}}{dt}, \quad (1)$$

where  $\gamma$  and  $\alpha$  are the gyromagnetic ratio and the Gilbert damping constant, respectively. The vector  $\mathbf{p}$  is a unit vector pointing along the direction of the spin polarization. In typical two-terminal devices made of a magnetic tunnel junction, current flows perpendicular to the plane [20–27,29,30]. Under such circumstances,  $\mathbf{p}$  is parallel to the magnetization of the reference layer. In three-terminal devices that consist of a heavy metal layer with large spin-orbit interaction and a magnetic tunnel junction [31–35,52–60],  $\mathbf{p}$  is often defined by the spin Hall effect of the heavy metal layer and/or the Rashba-Edelstein effect. For both cases, we may set  $\mathbf{p} = \mathbf{e}_y$ , as shown in Fig. 1.

The effective magnetic field  $\mathbf{H}$  is associated with the energy density  $E$  via  $E = -M \int d\mathbf{m} \cdot \mathbf{H}$ , where  $M$  is the saturation magnetization. Note that the explicit form of  $\mathbf{H}$  depends on the system. For a perpendicularly magnetized free layer,  $\mathbf{H} = H_K m_z \mathbf{e}_z$ , where  $H_K (> 0)$  is the magnetic anisotropy field. In contrast,  $\mathbf{H} = H_K m_y \mathbf{e}_y - H_d m_z \mathbf{e}_z$  for in-plane magnetized ferromagnets, where  $H_d$  is an effective demagnetization field. In both cases, the minimum and saddle energy densities are  $E_{\min} = -MH_K/2$  and  $E_d = 0$ , respectively. For later discussion, we introduce a thermal stability factor defined as  $(E_d - E_{\min})V/(k_B T)$ , i.e.,

$$\Delta_0 = \frac{MH_K V}{2k_B T}, \quad (2)$$

where  $V$  is the volume of the ferromagnet,  $k_B$  is the Boltzmann constant, and  $T$  is temperature. The strength of the spin-transfer torque is

$$H_s = \frac{\hbar g J}{2e M d}, \quad (3)$$

where  $d$  is the thickness of the free layer. The factor  $g$  characterizes the angular dependence of the spin-transfer torque, and its explicit form depends on the system. In two-terminal devices,  $g$  is well described by the formula  $g = \eta/(1 + \lambda \mathbf{m} \cdot \mathbf{p})$  [1,3], where  $\eta$  and  $\lambda$  are constants. The factor  $\eta$  represents the spin polarization of the current. In experiments, it has been reported that spin-transfer torque near the antiparallel alignment of  $\mathbf{m}$  and  $\mathbf{p}$  is larger than that near the parallel alignment. The factor  $1 + \lambda \mathbf{m} \cdot \mathbf{p}$  in  $g$  describes such an angular dependence. For three-terminal devices in which the spin Hall effect is the origin of the spin-orbit torque,  $g$  is the effective spin Hall angle  $\vartheta$  and is a constant. Here we do not consider the angular dependence of the spin-orbit torque [61,62].

### B. Evaluation method of switching probability

First we show the magnetization dynamics obtained by numerical simulations. To study the switching probability

TABLE I. Parameters used in the numerical calculations.  $M$ , saturation magnetization;  $H_{K\perp}$ , interfacial magnetic anisotropy field;  $\gamma$ , gyromagnetic ratio;  $V$ , volume of the free layer;  $\vartheta$ , spin Hall angle of the W channel.

Quantity	Value
$M$	1540 emu/cm <sup>3</sup>
$H_{K\perp}$	11.554 kOe
$\gamma$	$1.764 \times 10^7$ rad/(Oe s)
$V$	$\pi \times 44 \times 131 \times 2\text{nm}^3$
$\vartheta$	-0.34

ity, we numerically solve the LLG equation by adding a random torque ( $-\gamma\mathbf{m} \times \mathbf{h}$ ) due to thermal fluctuation to the right-hand side of Eq. (1). The components  $h_i$  ( $i = x, y, z$ ) of the stochastic field  $\mathbf{h}$  in Cartesian coordinates satisfy the fluctuation-dissipation theorem [19] (see also Appendix A),

$$\langle h_i(t)h_j(t') \rangle = \frac{2\alpha k_B T}{\gamma M V} \delta_{ij} \delta(t - t'). \quad (4)$$

In the numerical simulations, we focus on three-terminal devices with in-plane magnetized ferromagnets [33–35], where the effective magnetic field is given by  $\mathbf{H} = 4\pi M(N_x - N_y)m_y\mathbf{e}_y + [H_{K\perp} - 4\pi M(N_z - N_x)]m_z\mathbf{e}_z$ . The in-plane magnetic anisotropy field  $H_K$  is defined by the shape magnetic anisotropy field  $4\pi M(N_x - N_y)$ , where  $N_i$  ( $i = x, y, z$ ) is the demagnetization coefficient. The perpendicular magnetic anisotropy field  $-H_d$  consists of interfacial magnetic anisotropy field  $H_{K\perp}$  and shape magnetic anisotropy field  $-4\pi M(N_z - N_x)$ . The values of the parameters, shown in Table I are representative of a three-terminal device based on W/CoFeB/MgO [33–35] (see also Sec. III). The demagnetization coefficients estimated from the shape of the elliptic pillar are  $N_x \simeq 0.0420$ ,  $N_y \simeq 0.0089$ , and  $N_z \simeq 0.9491$  [63]. The current density  $J$  represents the current flow within the heavy metal layer.

Since the spin Hall angle of tungsten is negative, positive current induces magnetization to switch from  $-y$  to  $+y$  direction. We set the initial state of the magnetization to be  $\mathbf{m} = -\mathbf{e}_y$ , and solve the LLG equation under the influence of random field for 10 ns so that the magnetization is directed around the  $y$  axis (current is off during this period). From  $t = 10$  ns to  $t = 10 + t_p$  ns, the LLG equation with current and thermal fluctuation is solved, where  $t_p$  is the pulse width of the current. After that, the LLG equation with thermal fluctuation and without current is solved from  $t = 10 + t_p$  ns to  $t = 20 + t_p$  ns to stabilize the final state of the magnetization. When  $m_y$  at  $t = 20 + t_p$  ns is negative (positive), we regard the trial as nonswitched (switched). The LLG equation was solved by the fourth-order Runge-Kutta scheme with the time increment of  $\Delta t = 1$  ps.

Figures 2(a) and 2(b) are examples of nonswitched and switched trials, where  $\alpha = 0.033$ ,  $t_p = 3$  ns, and  $J$  is (a) 40 MA/cm<sup>2</sup> and (b) 60 MA/cm<sup>2</sup>. In Fig. 2(a), before passing the current ( $t < 10$  ns), the magnetization deviates slightly from the  $y$  axis randomly due to thermal fluctuation. The deviation increases when the current is passed ( $10 \leq t \leq 13$  ns). If  $J$  is small [Fig. 2(a)], however, the magnetization cannot escape from the negative  $y$  region. In contrast, the magnetization can switch to the positive  $y$  region when  $J$  is large, as shown in Fig. 2(b). We repeat such numerical simulations  $10^3$  times for each current density to obtain the switching probability (see also Appendix B).

Figure 2(c) shows an example of the switching probability  $P$  plotted as a function of  $J$ . The switching probability  $P$  shows an abrupt increase from 0 to 1 when  $J \sim 45$ –55 MA/cm<sup>2</sup>. It is interesting to note that the rate of change in  $P$  in the low and large current regions is different: here  $P$  changes rapidly in the low current region. Mathematically,  $|dP/dJ|$  near  $P = 0$  is larger than that near  $P = 1$ . This behavior is similar to what was observed in the experiments of an in-plane magnetized ferromagnet [9], as well as the numerical simulations of a perpendicularly magnetized ferromagnet [38] in the dynamical switching regime, while an opposite behavior was observed for the switching in the thermally activated regime [43]. In the following, we

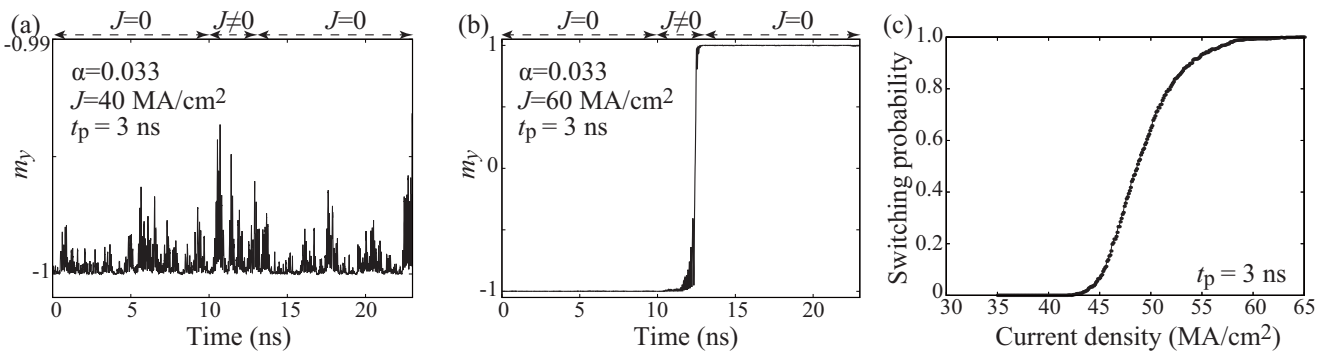


FIG. 2. Examples of the time evolution of  $m_y$  for current density  $J$  of (a) 40 and (b) 60 MA/cm<sup>2</sup>,  $\alpha = 0.033$ , and  $t_p = 3$  ns. The current density is turned on ( $J \neq 0$ ) after solving the LLG equation without current for 10 ns to make the initial state distributed around the  $y$  axis. After  $t = 10 + t_p$  ns, the LLG equation without current is solved for 10 ns to stabilize the final state. (c) An example of the switching probability for  $\alpha = 0.033$  and  $t_p = 3$  ns.

will derive a theoretical formula of the switching probability, which reproduces such characteristics.

### C. Device structures to which the formulation can be applied

Before deriving the formula of the switching probability, let us discuss the device structures to which the present work can be applied since it is related to the approximation used in the formulation.

The LLG equation is a nonlinear equation of two variables and, in general, hard to solve exactly. Therefore, we use the following assumptions to reduce the LLG equation to an equation of motion with one variable. The magnetization switching induced by the spin-transfer torque is classified into two types. First, the switching occurs as a result of the competition between the damping torque and the spin-transfer torque. In this type, the precession torque,  $-\gamma \mathbf{m} \times \mathbf{H}$ , dominates in the LLG equation. Accordingly, the switching accompanies precession. The second type is that the switching occurs when the spin-transfer torque overcomes the precession torque during a time shorter than the precession period around the stable state. For this type, the switching occurs without precession. These types can be distinguished by, for example, the formula of the threshold current for switching; the threshold current of the first type is proportional to the damping constant [12,36,45,64,65], whereas that of the second type is approximately independent of the damping constant [66–70].

The switching probability formula derived below can be applied to the first type, where the switching accompanies precession. The dynamical and thermally activated switchings discussed in this paper belong to this type, where the current density  $J$  is larger (smaller) than the threshold value  $J^*$  for the dynamical (thermally activated) switching, as noted in Sec. I. Note that the precession torque,  $-\gamma \mathbf{m} \times \mathbf{H}$ , induces a precession on a constant energy curve determined by the value of  $E$ . Under such circumstances, we may average the LLG equation with respect to the phase of the constant energy curve. As a result, the LLG equation is reduced to a one-variable differential equation. Such an approximation has been used in the analyses of the switching in the thermally activated regime and auto-oscillations [39,42,44–47,71].

Whether the switching occurs with or without the precession depends on various factors, such as the directions of the spin polarization, the easy axis of ferromagnets, the external magnetic field, and the angular dependence of the spin-transfer torque. For example, when the spin polarization has a projection along the easy-axis direction, the switching often accompanies precession [44–46]. In contrast, when the spin polarization is orthogonal to the easy axis, precessional dynamics can be excited in two-terminal devices [72] while the switching occurs without the precession in three-terminal devices [66,73]. The difference between the two devices arises from the difference in the angular dependence of the spin-transfer torque. In typical two-terminal devices (e.g., magnetic tunnel junctions), the spin polarization, defined by the magnetization in the reference layer, is parallel to the easy axis of the free layer. The formula derived here is therefore applicable to a wide range of two-terminal devices. For three-terminal devices (driven by spin-orbit torque), the so-called type-Y

structure [73] is classified as the first type, where the switching accompanies precession. In such a structure, the magnetic easy axis of the free layer is parallel to the spin polarization of the spin current, both of which point along the  $y$ -axis, which is transverse to the current flow direction (current flows along the  $x$ -axis). In the other types of three-terminal devices, known as type-X and type-Z, the switching does not accompany precession [66–69]. The switching probability formula for type-Z was derived in Ref. [67]. The formula derived here is applicable to type-Y and type-XY (easy axis points in between the  $x$ - and  $y$ -axes) devices [33–35,74].

### D. Solution of the LLG equation at zero temperature

When the switching accompanies precession, the LLG equation can be averaged on a constant energy curve. The trajectory of the precession is distinguished by the value of the energy density  $E$ . The LLG equation averaged over constant energy curves becomes (see also Appendix C)

$$\frac{dE}{dt} = \frac{1}{\tau(E)} [\mathcal{W}_\alpha(E) + \mathcal{W}_s(E)], \quad (5)$$

where  $\tau(E)$  is the precession period on a constant energy curve of  $E$ , while  $\mathcal{W}_\alpha(E)$  and  $\mathcal{W}_s(E)$  are the dissipation due to the damping torque and the work done by the spin-transfer torque during a precession.  $\mathcal{W}_\alpha(E)$  and  $\mathcal{W}_s(E)$  are defined as

$$\mathcal{W}_\alpha(E) = -\alpha\gamma M \oint dt [\mathbf{H}^2 - (\mathbf{m} \cdot \mathbf{H})^2], \quad (6)$$

$$\mathcal{W}_s(E) = \gamma M \oint dt H_s [\mathbf{p} \cdot \mathbf{H} - (\mathbf{m} \cdot \mathbf{p})(\mathbf{m} \cdot \mathbf{H})]. \quad (7)$$

The integrals in Eqs. (6) and (7) are calculated by substituting the solution of the Landau-Lifshitz (LL) equation,  $d\mathbf{m}/dt = -\gamma \mathbf{m} \times \mathbf{H}$ , into the integrands. Recall that the effective magnetic field of an in-plane magnetized ferromagnet was given by  $\mathbf{H} = H_K m_y \mathbf{e}_y - H_d m_z \mathbf{e}_z$ , where the energy density is  $E = -(MH_K/2)m_y^2 + (MH_d/2)m_z^2$ . It is useful for later discussion to derive the explicit forms of  $\mathcal{W}_\alpha$  and  $\mathcal{W}_s$  for the in-plane magnetized system [75],

$$\mathcal{W}_\alpha(E) = -4\alpha M \sqrt{\frac{H_d - 2E/M}{H_K}} \left[ \frac{2E}{M} \mathbf{K}(k) + H_K \mathbf{E}(k) \right], \quad (8)$$

$$\mathcal{W}_s = \frac{\pi \hbar \vartheta J (H_K + 2E/M)}{ed \sqrt{H_K (H_K + H_d)}}, \quad (9)$$

where  $\mathbf{K}(k) = \int_0^{\pi/2} d\phi / \sqrt{1 - k^2 \sin^2 \phi}$  and  $\mathbf{E}(k) = \int_0^{\pi/2} d\phi \sqrt{1 - k^2 \sin^2 \phi}$  are the first and second kind of complete elliptic integral with the modulus  $k$ ,

$$k = \sqrt{\frac{H_d (H_K + 2E/M)}{H_K (H_d - 2E/M)}}. \quad (10)$$

The precession period  $f(E) = 1/\tau(E)$  is

$$f(E) = \frac{\gamma \sqrt{H_K (H_d - 2E/M)}}{4\mathbf{K}(k)}, \quad (11)$$

which reproduces the ferromagnetic resonance (FMR) frequency,  $f_{\text{FMR}} = \gamma \sqrt{H_K (H_K + H_d)} / (2\pi)$ , in the limit of the minimum energy density,  $E \rightarrow E_{\text{min}}$ .

From Eq. (5), we find that

$$t_s = \int_{E_i}^{E_f} \frac{dE}{[\mathcal{W}_\alpha(E) + \mathcal{W}_s(E)]/\tau(E)}, \quad (12)$$

where  $t_s$  is the time necessary to move the magnetization from an initial energy state  $E_i$  to a final energy state  $E_f$ . Since we are interested in magnetization switching,  $E_i$  should be close to the minimum energy state  $E_{\min}$ , whereas  $E_f$  should be the saddle point energy,  $E_d$ . As can be seen in Eqs. (8) and (9), the integrand in Eq. (12) is a nonlinear function of  $E$ , and thus calculation of the integral is difficult in general. It should be noted that both  $\mathcal{W}_\alpha$  and  $\mathcal{W}_s$  often become zero in the limit of  $E \rightarrow E_{\min}$ . In fact, Eqs. (8) and (9), as well as the modulus  $k$  given by Eq. (10), become zero when  $E = E_{\min}$  for device structures and effective magnetic fields used in Sec. II B. Therefore, the lower limit  $E_i$  of the integral in Eq. (12) should be slightly larger than the minimum energy  $E_{\min}$ . It should also be noted that the integrand in Eq. (12) becomes large when the integration variable  $E$  is close to  $E_{\min}$ . Accordingly, using an approximation

$$\mathcal{W}_\alpha(E) + \mathcal{W}_s(E) \simeq \left[ \frac{d\mathcal{W}_\alpha(E)}{dE} + \frac{d\mathcal{W}_s(E)}{dE} \right]_{E=E_{\min}} (E - E_{\min}), \quad (13)$$

we notice that the integral in Eq. (12) can be approximately calculated as

$$t_s \simeq \frac{\tau(E_{\min})}{-[d\mathcal{W}_\alpha(E)/dE]_{E=E_{\min}}(J/J_c - 1)} \ln \frac{\Delta E}{\delta E}, \quad (14)$$

where  $\Delta E = E_d - E_{\min}$  and  $\delta E = E_i - E_{\min}$ . The critical current density,  $J_c$ , which is the minimum current density to destabilize the magnetization near the stable state, is defined from the following equation (see also Appendix D):

$$\frac{J}{J_c} = - \frac{d\mathcal{W}_s/dE}{d\mathcal{W}_\alpha/dE} \Big|_{E=E_{\min}}. \quad (15)$$

Using Eqs. (8) and (9), the explicit form of  $J_c$  in the in-plane magnetized system is

$$J_c = \frac{2\alpha eMd}{\hbar\vartheta} \left( H_K + \frac{H_d}{2} \right), \quad (16)$$

which is consistent with the critical current density obtained from the linearized LLG equation [36,64]. We should note that the critical current density  $J_c$  does not determine the threshold for switching. The threshold current density for the magnetization switching is (see also Appendix D) [45]

$$J^* = \frac{4\alpha eMd}{\pi \hbar\vartheta} \sqrt{H_d(H_K + H_d)}. \quad (17)$$

Note that the threshold current density is defined as the maximum current density satisfying  $\mathcal{W}_\alpha(E) + \mathcal{W}_s(E) = 0$  for  $E$  in the range of  $E_{\min} \leq E \leq E_d$ . For in-plane magnetized systems,  $J^*$  corresponds to the current density when  $E = E_d$ . At zero temperature, when  $J/J_c < 1$ , the magnetization relaxes to the minimum energy state, while an auto-oscillation on a trajectory close to the constant energy curve is excited when  $J/J_c \geq 1$  and  $J/J^* < 1$ . The magnetization switching without thermal activation occurs when  $J/J^* \geq 1$ . Therefore, the dynamical and thermally activated switching regimes are observed when  $J/J^* > 1$  and  $J/J^* < 1$ , respectively.

We would like to emphasize here that  $J^*$  is the minimum current density necessary to switch the magnetization when the duration of the applied current is infinite (i.e.,  $t \rightarrow \infty$ ). When the current pulse width is finite, a current density larger than  $J^*$  is required, as will be discussed below (Sec. II G).

For in-plane magnetized ferromagnets, the factor  $d\mathcal{W}_\alpha/dE$  in Eq. (14) reads

$$\frac{d\mathcal{W}_\alpha}{dE} \Big|_{E=E_{\min}} = - \frac{2\pi\alpha(2H_K + H_d)}{\sqrt{H_K(H_K + H_d)}}, \quad (18)$$

while  $\tau(E_{\min}) = (2\pi)/[\gamma\sqrt{H_K(H_K + H_d)}]$ . Therefore, Eq. (14) becomes

$$t_s = \frac{\ln(\Delta E/\delta E)}{2\pi \Delta f (J/J_c - 1)}, \quad (19)$$

where  $\Delta f$  is the FMR linewidth defined as

$$\Delta f = - \frac{1}{2\pi \tau(E_{\min})} \frac{d\mathcal{W}_\alpha(E)}{dE} \Big|_{E=E_{\min}}, \quad (20)$$

and is explicitly given for the in-plane magnetized ferromagnet as [76]

$$\Delta f = \frac{\alpha\gamma}{2\pi} (2H_K + H_d). \quad (21)$$

Equation (19) is the time necessary to switch the magnetization from the initial state  $E_i = E_{\min} + \delta E$  to the saddle point by the spin-transfer torque with the current density of  $J$ . We note that Eq. (19) is a generalization of the relation between the current density and the switching time,  $t_s \propto 1/[(J/J_c) - 1]$ , obtained in axially symmetric systems [36]. While the relation has been empirically applied to the in-plane magnetized system [73], the derivation shown above guarantees its validity.

### E. Switching probability formula

In the dynamical switching regime, the principal role of thermal fluctuation is to randomly distribute the initial state [36,37]. The distribution of the initial state before application of current is given by the Boltzmann distribution,

$$P_B(E) = \frac{\exp[-(E - E_{\min})V/(k_B T)]}{k_B T (1 - e^{-\Delta_0})}, \quad (22)$$

where  $\Delta_0 = (E_d - E_{\min})V/(k_B T) = \Delta EV/(k_B T)$ . The Boltzmann distribution is normalized as  $\int_{E_{\min}}^{E_d} dE P_B = 1$ . Note that  $E$  in Eq. (22) differs from  $E_i$  in Eq. (19). The variable  $E$  in Eq. (22) is in the range of  $E_{\min} \leq E \leq E_d$ , and  $P_B(E)dE$  gives the probability to find the energy of the initial state at  $E$  (before passing current). The energy density  $E_i$ , on the other hand, is the initial energy of the system after the current is passed and it has a certain value.

Let us now discuss the switching probability when the duration of the applied current is finite. As in the experiments in Refs. [33–35], we assume that a current pulse of length  $t_p$  is applied to the system. We assume that thermal fluctuation plays a minor role during the switching because we are interested in a fast switching process (i.e., short current pulses). For a current pulse, we replace  $t_s$  in Eq. (19) with a pulse width  $t_p$ . Recall that Eq. (19) provides the switching time  $t_s$  when the initial state is at  $E_i$  and the current density

is  $J$ . With  $t_s$  replaced with  $t_p$ , Eq. (19) can be regarded as the equation that determines the value of  $E_i$  required to move the magnetization to the saddle point at  $t = t_p$ . When the initial state  $E$  in Eq. (22) has an energy larger than this value of  $E_i$ , the magnetization can switch its direction during a time shorter than  $t_p$ . This is because such an initial state is closer to the saddle point than the state of  $E_i$ , and thermal activation during the switching process is assumed to be negligible. Accordingly, the switching probability by current pulses with pulse width  $t_p$  and current density  $J$  is given as the integral of the initial distribution with the energy density larger than  $E_i$ , i.e.,

$$P = \int_{E_i}^{E_d} dE P_B(E) = \frac{\exp\{-\Delta_0 \exp[-2\pi \Delta f t_p (\frac{J}{J_c} - 1)]\} - \exp(-\Delta_0)}{1 - \exp(-\Delta_0)}. \quad (23)$$

Equation (23) is the switching probability in the dynamical regime, and it is the main result in this work. We note that Eq. (23) includes three parameters, namely the thermal stability factor  $\Delta_0$ , the FMR linewidth  $\Delta f$ , and the critical current density  $J_c$ . While we derived the theoretical formulas of these parameters for the in-plane magnetized systems, Eq. (23) is applicable to any devices mentioned in Sec. II C when the explicit forms of these parameters are replaced appropriately, according to their definitions.

The error rate of magnetization switching, defined as  $ER = 1 - P$ , is often used to characterize the device quality [25,37]. Assuming that  $\Delta_0 \gg 1$ , the error rate for  $J/J_c \gg 1$  estimated from Eq. (23) becomes

$$ER \simeq \Delta_0 \exp\left[-2\pi \Delta f t_p \left(\frac{J}{J_c} - 1\right)\right]. \quad (24)$$

#### F. Approximations used in the derivation of the switching probability formula

In Sec. II G, we will investigate the validity of Eq. (23) through comparison with numerical simulations. Before doing so, here let us discuss the applicability of the formula. Note that there are mainly two approximations made in the derivation of Eq. (23).

First, we assumed that the switching time is dominated by the time needed to escape from the near minimum energy state. This assumption can be seen in Eq. (13), where we expanded the integrand in Eq. (12) around the minimum energy state and neglected the higher-order terms of  $(E - E_{\min})$ . In reality, however, a finite time is necessary for the switching after escaping from the initial state. Accordingly, the time  $t$  given by Eq. (19) is shorter than the exact value of the switching time. This approximation also provides an inaccurate scale of the current, that is, Eq. (19) includes  $J_c$ , not  $J^*$ , although  $J_c$  is not the threshold current for the switching for the in-plane magnetized system.

The second approximation is that the effect of the thermal activation is included in the initial state only. This assumption is valid when the switching occurs in a short time. In reality, thermal fluctuation during the switching induces an active motion of the magnetization.

Despite these approximations, we will show that Eq. (23) agrees well with the results obtained from numerical simulations. We consider this is related to the fact that the two assumptions play opposite roles. The first approximation causes the switching probability estimated by the formula to reach  $P = 1$  faster than the exact solution (numerical simulations) of the LLG equation due to the following reason. If the magnetization moves sufficiently away from the stable state but cannot arrive at the saddle point of the energy, the event should be classified as “not-switched.” However, Eq. (23) defines such an event as “switching” because the formula only focuses on whether the magnetization escapes from the minimum energy state. Accordingly, the first approximation leads to faster saturation of the probability compared with the numerical simulations. The second assumption results in the switching probability to saturate slower than the exact solution since the approximation neglects the thermal activation during the switching. The roles of these approximations will be clarified in the next section.

#### G. Comparison with numerical simulations

Now let us get back to discussing the results of the numerical simulations and compare them with the switching probability formula.

Figure 3 summarizes the switching probability of in-plane magnetized ferromagnets described in Sec. II B, where the pulse width  $t_p$  is (a) 1, (b) 3, (c) 4, (d) 5, (e) 10, (f) 20, (g) 30, and (h) 50 ns. The damping constant is  $\alpha = 0.033$  [34,35]. The dots are obtained from the numerical simulations, as in the case of Fig. 2(c), while the (green) solid line corresponds to the theoretical formula, Eq. (23). The values of the parameters used in Eq. (23) are  $\Delta_0 = 431$ ,  $\Delta f = 674$  MHz, and  $|J_c| = 33.0$  MA/cm<sup>2</sup>. The large  $\Delta_0$  used here reflects the large area of the nanopillar used in the experiments; see Sec. III A. Note that  $|J^*| = 36.5$  MA/cm<sup>2</sup>. The switching, therefore, occurs in the dynamical regime ( $J/J^* > 1$ ) for the pulse widths from  $t_p = 1$  to 5 ns, while the switching for  $10 \leq t_p \leq 50$  ns is in an intermediate regime between the dynamical and thermally activated switching. The transition width of the switching probability decreases with increasing pulse width, which is opposite to what is expected for magnetization switching in the thermally activated regime [77].

We note that the formula given by Eq. (23) quantitatively reproduces the results of the numerical simulations. In addition, the formula reproduces the characteristic described in Sec. II B, i.e.,  $|dP/dJ|$  near  $P = 0$  is larger than that near  $P = 1$  (for shorter pulses). We notice that the switching probability obtained by the numerical simulations saturates faster than that predicted by the formula. This is because thermal fluctuation during the application of current, which is neglected in the formulation, prompts faster switching, as explained in Sec. III F.

When the damping constant is smaller, the stochastic field induced by thermal fluctuation decreases [see Eq. (4)] and its effect is reduced in the switching process. In Fig. 4, we summarize the switching probability when  $\alpha$  is reduced to 0.005. The pulse widths are the same as those in Fig. 3. In this case ( $\alpha = 0.005$ ),  $|J_c|$  and  $|J^*|$  are 5.0 and 5.5 MA/cm<sup>2</sup>,

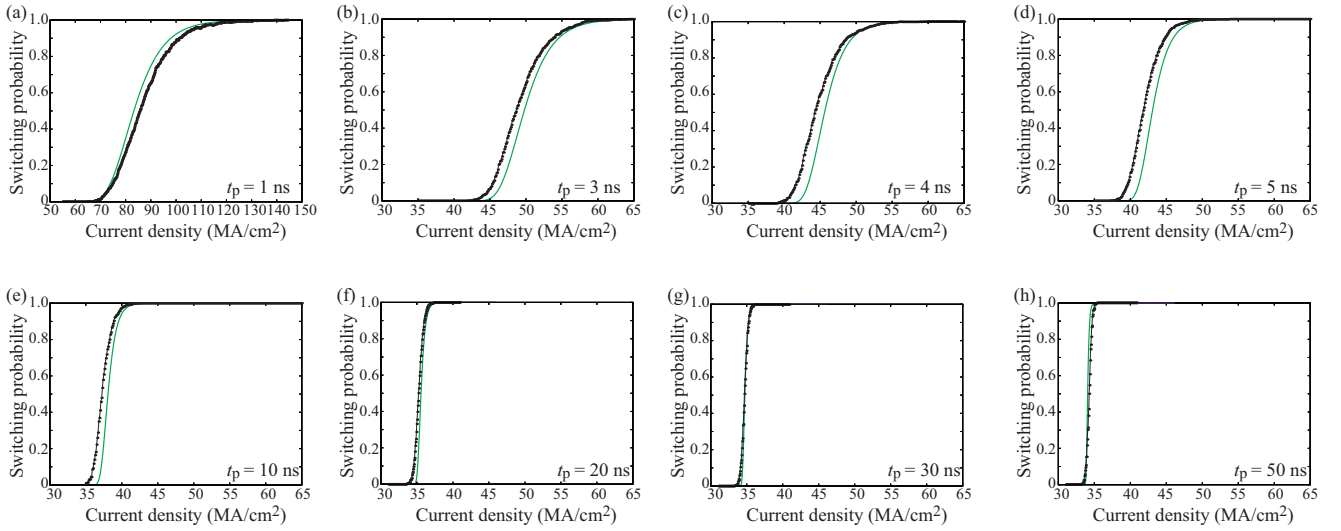


FIG. 3. Black dots represent the switching probability obtained from the numerical simulations of the LLG equation for pulse width  $t_p$  of (a) 1, (b) 3, (c) 4, (d) 5, (e) 10, (f) 20, (g) 30, and (h) 50 ns. The green solid lines are the switching probability calculated using Eq. (23). The damping constant  $\alpha$  is 0.033.

respectively, while  $\Delta f = 102$  MHz. As expected, the difference between the numerical and theoretical results becomes small. We also notice that the switching probability formula saturates faster than that of the numerical simulations when the pulse width is small. This is because the switching time estimated by Eq. (19) is faster than the real switching time, as explained in Sec. II F.

#### H. Comparison with previous works

We emphasize that Eq. (23) is a generalization of the switching probability formula derived for the perpendicularly magnetized system and has a wide applicability. Here, let us briefly summarize the results from previous works and compare them with the present work.

We first discuss a perpendicularly magnetized system. To describe such a system in our formalism, we simply need to neglect terms related to  $H_d$  and regard  $H_K$  as a net perpendicular magnetic anisotropy field. This results in substituting the following relations into Eq. (23):  $2\pi\Delta f = 2\alpha\gamma H_K$  and  $J_c = [2\alpha eMd/(\hbar\vartheta)]H_K$ .

The perpendicularly magnetized ferromagnet has an axial symmetry along the easy axis. Due to the higher symmetry of the system, the magnetization equation of motion depends on the tilt angle from the easy axis ( $\theta$ ) only. Without averaging over the energy states discussed in Sec. II D, the equation of motion reads

$$\frac{d\theta}{dt} = -\alpha\gamma H_K \sin\theta \cos\theta + \gamma H_s \sin\theta. \quad (25)$$

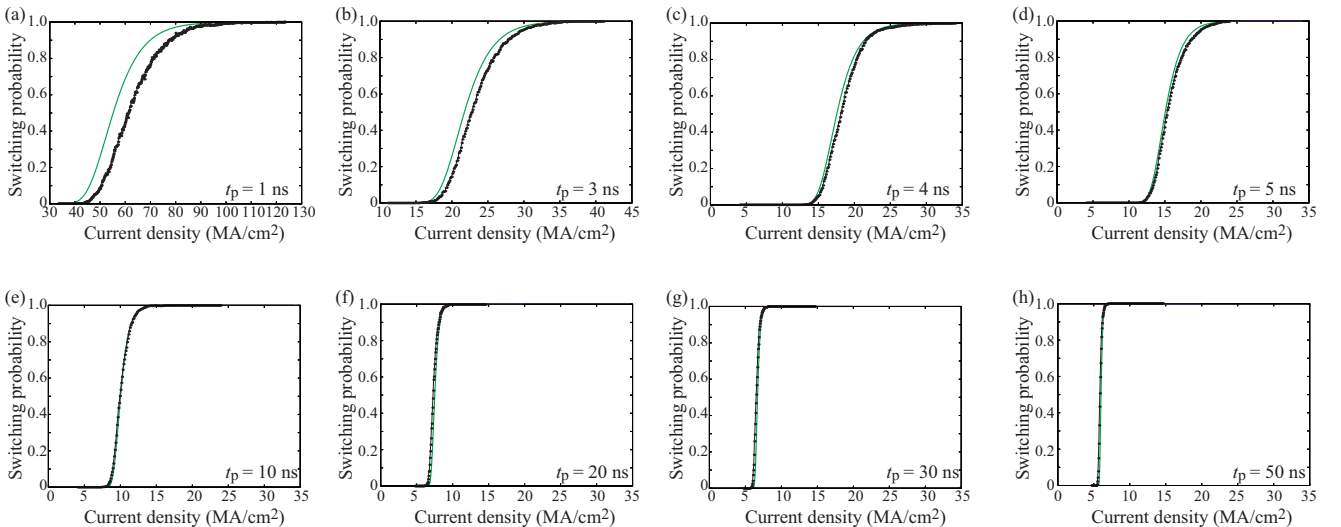


FIG. 4. Black dots represent the switching probability obtained from the numerical simulations of the LLG equation for pulse width  $t_p$  of (a) 1, (b) 3, (c) 4, (d) 5, (e) 10, (f) 20, (g) 30, and (h) 50 ns. The green solid lines are the switching probability calculated using Eq. (23). The damping constant  $\alpha$  is 0.005.

These features enabled the authors of Refs. [24,25,36,37] to derive the switching probability formula for the perpendicularly magnetized system with a few approximations. There are, however, a few differences among the previous works, although they focus on the same system.

For example, both Refs. [24,25] and Refs. [36,37] found that the switching probability of the perpendicularly magnetized system is well described by a formula,

$$P \propto \exp \left\{ -F(J)\Delta_0 \exp \left[ -2\pi \Delta f t_p \left( \frac{J}{J_c} - 1 \right) \right] \right\}, \quad (26)$$

where  $2\pi \Delta f = 2\alpha\gamma H_K$  and  $J_c = [2\alpha eMd/(\hbar\vartheta)]H_K$  (these forms are the same as those derived by our formalism). In the following, we discuss details of the derivation of Eq. (26). First, note that the formulas in Refs. [24,25,36,37] do not satisfy  $P(t=0) = 0$ . [ $P(t=0)$  might be sufficiently close to zero when  $\Delta_0$  is large.] This is rather unphysical since the state at  $t=0$  should be at the initial state, thus  $P$  must be zero. Our formula, Eq. (23), satisfies  $P(t=0) = 0$ , independent of the value of  $\Delta_0$ .

The factor  $F(J)$  in Eq. (26) is a constant in Refs. [36,37] while it is a function of the current density in Refs. [24,25]. The difference is related to the approximation they used, as shown below. For the perpendicularly magnetized system, we found from Eq. (25) that the integral corresponding to Eq. (12) becomes

$$t_s = \int \frac{d\theta}{\alpha\gamma H_K \sin \theta [(J/J_c) - \cos \theta]}, \quad (27)$$

where  $J_c = [2\alpha eMd/(\hbar g)]H_K$  is the critical current density of the perpendicularly magnetized ferromagnet. Reference [36] performs the integral with the approximations  $\sin \theta \simeq \theta$  and  $\cos \theta \simeq 1$ , and obtains

$$t_s = \frac{\ln[\pi/(2\delta\theta)]}{\alpha\gamma H_K [(J/J_c) - 1]}, \quad (28)$$

where  $\delta\theta$  is the tilted angle of the initial state while  $\pi/2$  corresponds to the angle of the saddle point. In contrast, Refs. [24,25] performed the integral without using such approximations and obtained

$$\begin{aligned} & \frac{1}{a+1} \ln \cos \frac{\delta\theta}{2} - \frac{1}{a-1} \ln \sin \frac{\delta\theta}{2} + \frac{1}{a^2-1} \ln \frac{a - \cos \delta\theta}{2a} \\ & = \alpha\gamma H_K t_s, \end{aligned} \quad (29)$$

where  $a = J/J_c$  is the notation used in Ref. [25]. Assuming  $\delta\theta \ll 1$ , Ref. [25] obtained

$$t_s = -\frac{1}{\alpha\gamma H_K (a-1)} \ln \left[ \frac{\delta\theta}{2} \left( \frac{2a}{a-1} \right)^{1/(a+1)} \right]. \quad (30)$$

Equations (28) and (30) can be summarized as

$$t_s = \frac{\ln(G/\delta\theta)}{\alpha H_K [(J/J_c) - 1]}, \quad (31)$$

where  $G = \pi/2$  in Eq. (28) and  $G = 2[2a/(a-1)]^{-1/(a+1)}$  in Eq. (30). From Eq. (31), one finds

$$\delta\theta = G \exp \left[ -\alpha\gamma H_K t_s \left( \frac{J}{J_c} - 1 \right) \right]. \quad (32)$$

The Boltzmann distribution for the perpendicularly magnetized ferromagnets is given by  $P_B \propto e^{\Delta_0 \cos^2 \theta}$ . Therefore, the switching probability is given by

$$P \propto \int_{\delta\theta}^{\pi/2} d\theta \sin \theta P_B \simeq \int_{\delta\theta}^{\infty} d\theta \theta e^{\Delta_0(1-\theta^2)} \propto e^{-\Delta_0 \delta\theta^2}, \quad (33)$$

where we use the approximation of  $\theta \ll 1$ . Substituting Eq. (32) into Eq. (33) and noting that  $2\pi \Delta f = 2\alpha\gamma H_K$ , we obtain Eq. (26), where  $F = G^2$  is  $\pi^2/4$  in Refs. [36,37] and  $4[2a/(a-1)]^{-2/(a+1)}$  in Refs. [24,25]. As can be seen in these explanations, even in the perpendicularly magnetized system where the system has high symmetry and the LLG can be integrated exactly, the switching probability formulas can differ depending on the approximations used, which can be seen in the derivations of Eqs. (28) [36,37] and (30) [24,25].

In the case of the in-plane magnetized ferromagnet, it is difficult to integrate Eq. (12) exactly unless approximations such as Eq. (13) are used. Nevertheless, we showed in Figs. 3 and 4 that Eq. (23) qualitatively explains the switching probability of the in-plane magnetized ferromagnets. Moreover, we point out that this work shows the validity and the applicable range of the relation [Eq. (19)] between the switching time and the applied current density, which was derived for the perpendicularly magnetized system [24,25,36] and has been empirically applied to in-plane magnetized systems [73].

### I. Distinction between dynamical and thermally activated switching regimes

In previous works, the dynamical and thermally activated switching regimes have been distinguished by evaluating the switching current density as a function of pulse width [21,24,27,38]. This method, however, requires a systematic investigation of the switching probability over a wide range of pulse widths. Equation (23) implies another, relatively simple, method to distinguish the dynamical and thermally activated regimes.

The switching probability formula in the thermally activated regime is given by [19,39–47]

$$P = 1 - \exp \left\{ -f_a t_p \exp \left[ -\Delta_0 \left( 1 - \frac{J}{J_*} \right)^b \right] \right\}, \quad (34)$$

where  $f_a$  is an attempt frequency. The switching exponent  $b$  is 2 for perpendicularly magnetized ferromagnets [40–43] while it is close to 2 and depends on the material parameters for in-plane magnetized ferromagnets [45]. We notice that Eqs. (23) and (34) have a different symmetry with respect to the current.

The solid lines in Figs. 5(a) and 5(b) schematically show the switching probability in the dynamical and thermally activated regimes, obtained from Eqs. (23) and (34), respectively. We also show the probability density, defined as  $dP/dJ$ , by dashed lines. Note that the probability density is asymmetric with respect to the current density, and the asymmetry is opposite in the dynamical and thermally activated switching regimes. The probability density of the dynamical switching has a larger tail where current is larger than the peak position. In contrast, the probability density of the thermally activated switching has a larger tail in the lower current region. The shape of the probability density, therefore, provides direct



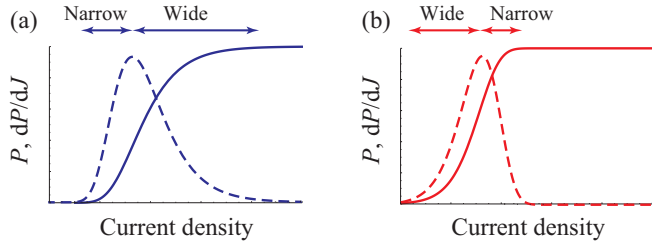


FIG. 5. Calculated switching probability  $P$  (solid lines) and the probability density  $dP/dJ$  (dashed lines) of (a) dynamical and (b) thermally activated switching regimes. The distribution of the probability density for the dynamical (thermally activated) switching is wider for the large (small) current region.

evidence of the switching regime, whether it is the dynamical or thermally activated regime.

As mentioned, the present model is applicable to the dynamical switching regime. In addition to the well-studied thermally activated regime, switching in an intermediate regime has been discussed recently [78]. The switching-time formulas of the thermally activated and dynamical regimes were combined with weights, and a gamma distribution function was used for fitting the switching probability. Although the approach is heuristic and empirical, it provides a connection between the two limits.

In general, the switching probability formula is obtained as a solution of the time-dependent Fokker-Planck equation [19]. Solving the Fokker-Planck equation exactly, however, is difficult, and approximations are necessary for deriving analytical formulas of the switching probability in different limits. Further studies are required to develop a comprehensive theory that can account for the switching probability over a wide range of parameters.

### III. EXPERIMENTAL ANALYSIS

In this section, we show experimental results from type-Y three-terminal devices (with in-plane magnetized ferromagnet) to study the applicability of the formula described above.

#### A. Device structure and magnetic properties

The three-terminal device consists of a W channel and a magnetic tunnel junction (MTJ) [34,35]. The MTJ is comprised of a bottom CoFeB (2) free layer and a CoFeB(2)/Ru(0.8)/CoFe(2)/IrMn(8.5)/Ru(2)/Ta(3) top reference layer separated by an MgO(1.8) barrier (thickness in nm). The film stack was postannealed at 250 °C for 3 h in an in-plane magnetic field over 1 T. As described in Sec. II B, the MTJ is patterned into an elliptic cylinder. The length of the ellipse's short and long axes is about 90 and 260 nm, respectively. The thickness of the W channel is 3 nm and its width is about 260 nm. The resistance of the W channel is about 2.2 k $\Omega$ .

A schematic illustration of the measurement setup is presented in Fig. 6(a). A constant voltage pulse generator and a 50  $\Omega$  load are connected to the W channel via the high-frequency port of the bias tees. The voltage pulse, with amplitude  $V_p$  and length  $t_p$ , supplies current to the W channel.

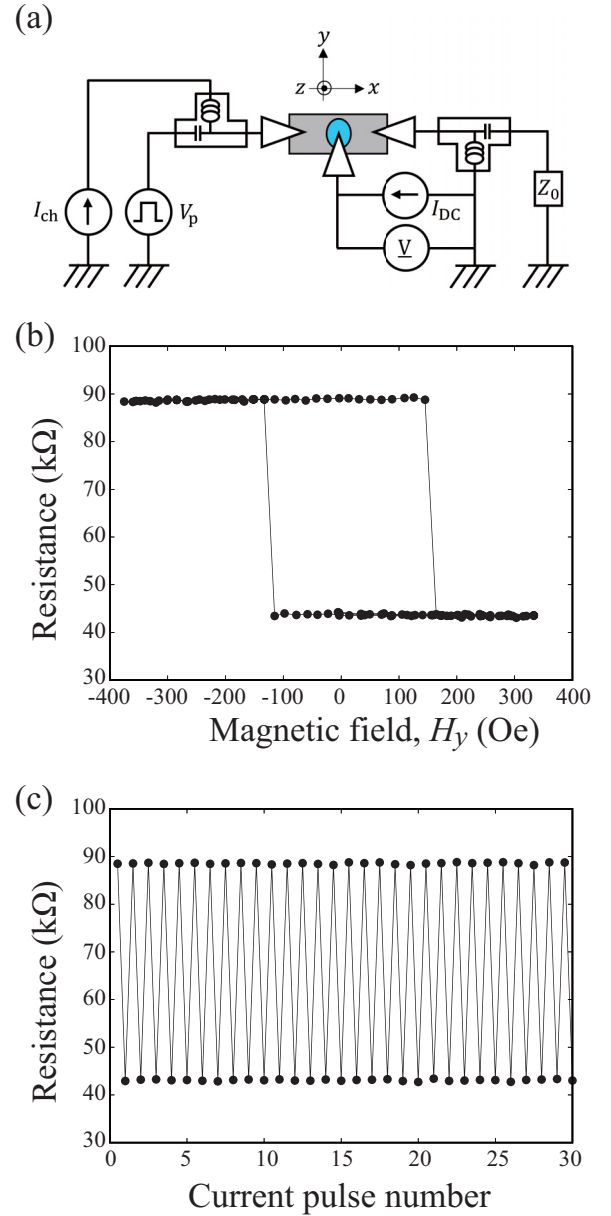


FIG. 6. (a) Schematic illustration of the measurement circuit, where  $Z_0$  represents a 50  $\Omega$  load. (b) Resistance of the MTJ as a function of an external magnetic field ( $H_y$ ) applied along the  $y$  direction. (c) Resistance of the MTJ as a function of pulse number. The high (low) resistance state corresponds to the initial (switched) state. A data set from the  $10^4$  measurements is shown.

The spin current generated in the W channel via the spin Hall effect diffuses into the free layer of the MTJ and exerts spin-transfer torque (or spin-orbit torque) on the magnetization. To read out the state of the MTJ, a small dc bias current  $I_{dc}$  is applied to the MTJ from the gate of the three-terminal device (i.e., the current source is connected to the MTJ reference layer). The dc ground is connected to the W channel via the low-frequency port of the bias tee. The resistance of the MTJ is monitored using a nanovoltmeter. A small sense current  $I_{ch}$  is applied to the W channel, via the low-frequency port of the bias tee, to monitor its resistance.  $I_{ch}$  is set to zero during

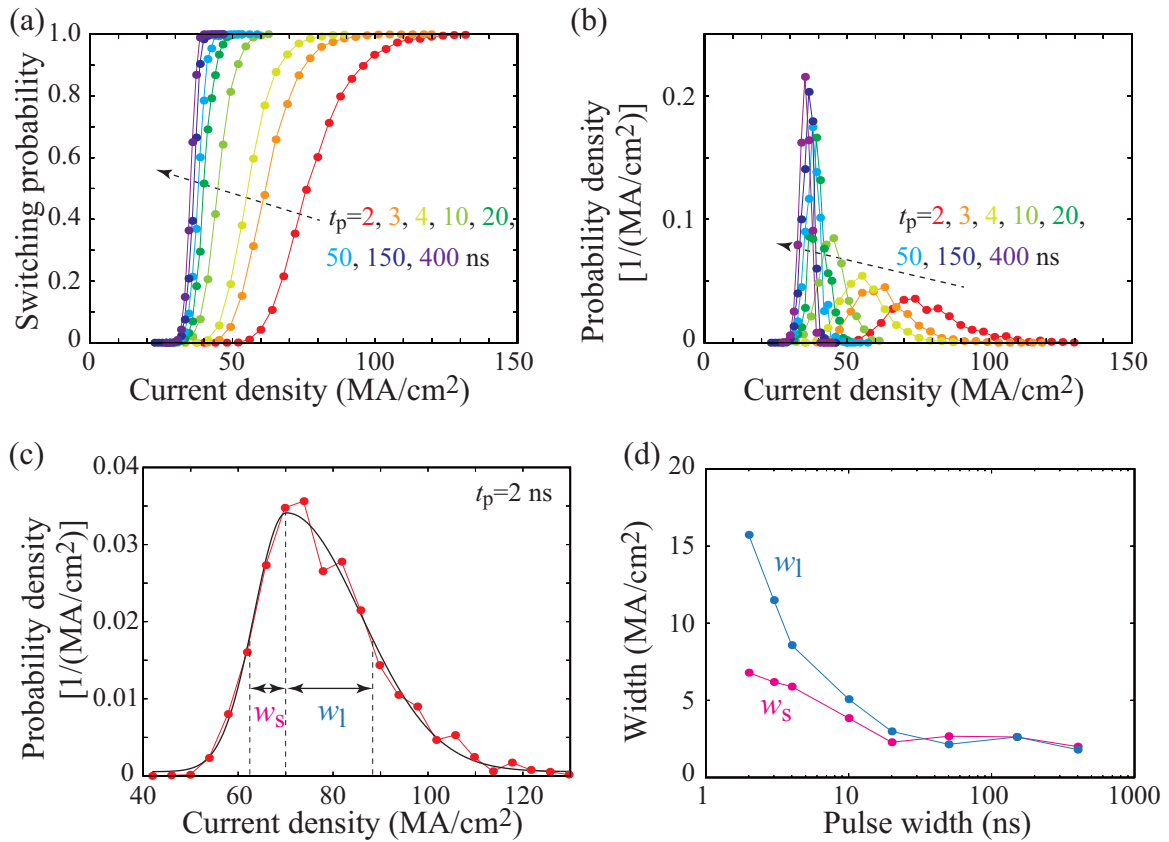


FIG. 7. (a) Switching probability,  $P$ , and (b) the probability density,  $dP/dJ$ , of the three-terminal device studied. The pulse widths are 2, 3, 4, 10, 20, 50, 150, and 400 ns from right to left. (c) An enlarged view of the probability density for the data with a pulse width of 2 ns. The solid black line shows the fitting result using a bi-Gaussian function.  $w_s$  and  $w_l$  are the fitting parameters defined as illustrated. (d) Dependences of  $w_s$  and  $w_l$  on the pulse width.

the MTJ resistance measurements. All measurements were performed at room temperature using a home-made transport measurement system.

Figure 6(b) shows the magnetic field dependence of the MTJ resistance of a typical three-terminal device. The field ( $H_y$ ) is applied along the magnetic easy axis of the MTJ free layer, i.e., along the  $y$  direction sketched in Fig. 1. Within the range of  $H_y$  applied, the magnetization direction of the reference layer does not change. The loop shown in Fig. 6(b) thus shows the hysteresis of the free-layer magnetization. The magnetoresistance ratio, defined as  $\Delta R/R_p$ , is 105%, where  $\Delta R \equiv R_{AP} - R_p$ , and  $R_{AP}$  and  $R_p$  are the resistance for the antiparallel and parallel states, respectively, of the magnetization configuration of the reference and free layers. The center of the loop in Fig. 6 is shifted from the origin  $H_y = 0$  due to the stray field from the reference layer, which is estimated to be about 11 Oe. The coercive field is about 140 Oe. The in-plane magnetic anisotropy field ( $H_K$ ), obtained from separate measurements, is about 560 Oe. The measured  $H_K$  is close to the shape magnetic anisotropy field estimated from the demagnetization factors of the elliptic pillar.

We study the probability of current-induced magnetization switching using the following procedure. The field is set to a value ( $H_y \sim 11$  Oe) that allows cancellation of the stray field from the reference layer. We first initialize the magnetic state of the free layer by applying a direct current

of 27 MA/cm<sup>2</sup> for 100 ms. From preliminary measurements, we find such a condition that allows initialization with little error. Next, a single voltage pulse from a pulse generator is applied to the W channel. The resistance of the MTJ is measured before and after the pulse application to study the magnetic state of the free layer. If the magnitude of the resistance change after the pulse application is more than 85% of  $\Delta R$  found in the hysteresis loop shown in Fig. 6(b), we assume the free-layer magnetization was switched. This process is repeated  $10^4$  times to obtain the switching probability. Here we show results where the initial state is the high resistance state (antiparallel alignment of the reference and free layer). Figure 6(c) shows an example of the measurements, where the pulse width and the current density are 20 ns and 49 MA/cm<sup>2</sup>, respectively. Current-induced magnetization switching is found for all trials shown. We have studied more than 10 devices and found similar characteristics in many of the devices. Representative results from a single device are presented here.

### B. Switching probability

Figure 7(a) summarizes the switching probabilities obtained using voltage pulses with widths of 2, 3, 4, 10, 20, 50, 150, and 400 ns. The current density that flows along the W channel is calculated from the pulse amplitude and the channel

resistance. The switching probability varies from 0 to 1 as the current density is increased (see also Appendix E for the accuracy of the evaluation on the switching probability). The current density at which the switching probability exceeds 0.5, defined as  $J_{50\%}$ , increases with a decreasing pulse width. The transition width of the switching also increases with a decreasing pulse width. These results are consistent with the numerical simulations (see Figs. 3 and 4), suggesting that the switching occurs in a dynamical switching regime.

In Fig. 7(b), we show the probability density, the current density derivative of the switching probability. The shape of the probability density varies as the pulse width is changed. As discussed in Sec. III, the dynamical and thermally activated switching regimes can be distinguished from the distribution of the probability density with respect to its peak. To analyze the shape of the probability density, we fit the data with a bi-Gaussian function. Figure 7(c) shows the probability density when the pulse width is set to 2 ns. The solid lines show the fitting result. We use three fitting parameters: widths  $w_s$  and  $w_l$ , as illustrated in Fig. 7(c), and the amplitude.  $w_s$  ( $w_l$ ) represents the width from the peak position to the lower (higher) current density to which the probability density is half of the peak value. When  $w_s < w_l$  ( $w_s > w_l$ ), the switching occurs in the dynamical (thermally activated) regime. Figure 7(d) summarizes the pulse width dependence of  $w_s$  and  $w_l$ . The results show that the dynamical switching regime dominates when the pulse width is shorter than  $\sim 20$  ns.

We note that previous studies have shown the means to distinguish the switching regime. In many cases, the averaged threshold switching current was measured over a wide range of pulse width [21,24,25,27]. In the dynamical switching regime, the switching current is inversely proportional to the pulse width, as can be seen in Eq. (19), while that in the thermally activated regime has a logarithmic dependence on the pulse width, as implied from Eq. (34). The present analysis and the associated experimental results, however, demonstrate that the switching regime can be directly identified from the shape of the switching probability. These findings would be useful for the analyses of the switching probability of two-terminal spin torque and three-terminal spin-orbit torque switching devices.

Note that the agreement we obtained between theory and experiment is qualitative. The lack of a quantitative agreement might be due to the limitation of the macrospin model. An incoherent magnetization rotation and/or creation of multiple domain structures might appear in the experimental sample. We keep the development of the model beyond the macrospin model as future work.

#### IV. CONCLUSION

In summary, current-induced magnetization switching of an in-plane magnetized ferromagnet in the dynamical switching regime was studied. A generalized formula of the switching probability was derived from the LLG equation. The formula includes three parameters: a thermal stability factor, linewidth of ferromagnetic resonance, and critical current density. A quantitative good agreement between the theory and numerical simulations was obtained, in particular, when the damping constant is small. The formula also reproduces

several characteristics found in the numerical simulations. For example, the transition width of the switching probability increases with decreasing pulse width. The probability density, i.e., the current density derivative of the switching probability, is asymmetric with respect to its peak when short current pulses are applied. The tail of the probability density for the higher current region increases as the pulse width is reduced. Such features have been identified in experiments where the magnetization switching probability of three-terminal spin-orbit torque switching devices is studied. From the analyses, we show that the asymmetric shape of the probability density is related to the switching regime: the tail is larger for the higher (lower) current region for the dynamical (thermally activated) switching regime. These results thus validate the formula developed and show that the shape analyses of the probability density provide straightforward means to identify the switching regime.

#### ACKNOWLEDGMENTS

This work was supported by funding from TDK Corporation. T.T. is grateful to Takehiko Yorozu for valuable discussion.

#### APPENDIX A: NUMERICAL TECHNIQUE ADDING THERMAL FLUCTUATIONS

In the numerical simulation, the random field is given by ( $i = x, y, z$ )

$$h_i(t) = \sqrt{\frac{2\alpha k_B T}{\gamma M V \Delta t}} \xi_i(t). \quad (\text{A1})$$

The time increment  $\Delta t$  is 1 ps, as mentioned. White noise  $\xi$  is defined from two random numbers,  $\zeta_a$  and  $\zeta_b$ , in the range of  $0 < \zeta_a, \zeta_b \leq 1$  by the Box-Muller transformation as  $\xi_a = \sqrt{-2 \ln \zeta_a} \sin(2\pi \zeta_b)$  and  $\xi_b = \sqrt{-2 \ln \zeta_a} \cos(2\pi \zeta_b)$ . We added Eq. (A1) to the magnetic field and solved the LLG equation numerically using the Runge-Kutta method. The method thus includes spurious drift terms [79] and belongs to the Stratonovic prescription. The contribution of the random torque to the time evolution of the magnetization is on the order of  $h_i \Delta t \propto \sqrt{\Delta t}$ .

#### APPENDIX B: ACCURACY OF THE SWITCHING PROBABILITY IN SIMULATION

As written in Sec. II B, the switching probability is numerically obtained from  $10^3$  trials using different random fields. One might be interested in the accuracy of this estimation. Figure 8(a) shows the switching probability obtained from 100 (blue), 200 (green), 500 (red), and 1000 (black) trials, where  $t_p = 1$  ns and  $\alpha = 0.033$ . The black line is identical to that shown in Fig. 3(a). As is evident, the switching probability shows larger scattering when the trial number is reduced. From this plot, the scattering is negligible when the trial number is set to  $10^3$ .

To evaluate the error, we repeat the simulations for the  $10^3$  trials 10 times with different random numbers. The average, minimum, and maximum values of the switching probability at each current density are extracted. The results are shown

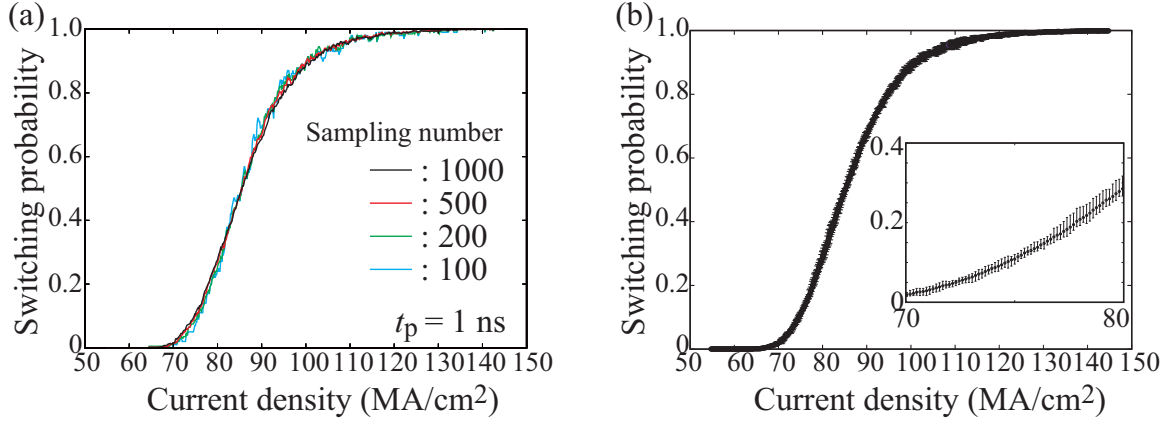


FIG. 8. The switching probability for  $t_p = 1$  ns and  $\alpha = 0.033$ . (a) The number of trials is changed as 100 (blue), 200 (green), 500 (red), and 1000 (black). (b) The averaged value of the switching probability, where the evaluation of the switching probability from  $10^3$  trials is repeated 10 times with different random numbers, and such 10 probabilities are averaged. The bars at each current density represent the difference in the maximum and minimum values in the 10 samplings. The inset shows an enlarged view in the current density range of  $70 \leq J \leq 80$  MA/cm $^2$ .

in Fig. 8(b). The error bars represent the difference of the maximum and minimum values of the switching probability. The error range is sufficiently small and allows comparison with the theoretical formula.

### APPENDIX C: AVERAGING TECHNIQUE OF THE LLG EQUATION

Here, we explain the averaging technique of the LLG equation over a constant energy curve. Note that the constant energy curve is a trajectory given as a solution of the Landau-Lifshitz (LL) equation,  $d\mathbf{m}/dt = -\gamma\mathbf{m} \times \mathbf{H}$ . Let us first investigate the solution of the LL equation for an in-plane magnetized system as an example [75]. Since the LL equation conserves the norm of the magnetization, i.e.,  $|\mathbf{m}| = 1$ , the energy density  $E = -(MH_K/2)m_y^2 + (MH_d/2)m_z^2$  can be rewritten as

$$m_z^2 + \frac{H_K}{H_K + H_d} m_x^2 = \frac{2E/M + H_K}{H_K + H_d}. \quad (\text{C1})$$

Thus,  $m_x$  and  $m_z$  can be expressed as  $m_x = (v'/v) \sin u$  and  $m_z = v' \cos u$  with  $v^2 = H_K/(H_K + H_d)$  and  $v'^2 = (2E/M + H_K)/(H_K + H_d)$ . Then, using the LL equation, we find that  $du/dt = (v/m_z)(dm_x/dt)$  becomes

$$\frac{du}{dt} = \gamma(H_K + H_d)vm_y. \quad (\text{C2})$$

Introducing a new variable  $w = \sin u$ , this equation becomes

$$\frac{dw}{\sqrt{(1-w^2)(1-k^2w^2)}} = \gamma(H_K + H_d)v\sqrt{1-v^2}dt, \quad (\text{C3})$$

where the modulus  $k$  is given by Eq. (10). The solution of  $w$  is given by the Jacobi elliptic function  $\text{sn}(y, k)$  with  $y = \gamma\sqrt{H_K(H_d - 2E/M)}t + \varphi_0$ , where the initial phase  $\varphi_0$  is determined by the initial condition. Recall that  $w$  relates to  $m_x$  via  $m_x = (v'/v)w$ . Introducing other Jacobi elliptic functions  $\text{cn}(y, k)$  and  $\text{dn}(y, k)$  that satisfy  $\text{sn}^2(y, k) + \text{cn}^2(y, k) = 1$  and

$\text{dn}^2(u, k) = \sqrt{1 - k^2\text{sn}^2(u, k)}$ , the solution of the LL equation for the in-plane magnetized system becomes

$$m_x = \sqrt{1 + \frac{2E}{MH_K}} \text{sn} \left[ \frac{4K(k)}{\tau(E)}t + \varphi_0, k \right], \quad (\text{C4})$$

$$m_y = \sqrt{\frac{H_d - 2E/M}{H_K + H_d}} \text{dn} \left[ \frac{4K(k)}{\tau(E)}t + \varphi_0, k \right], \quad (\text{C5})$$

$$m_z = \sqrt{\frac{H_K + 2E/M}{H_K + H_d}} \text{cn} \left[ \frac{4K(k)}{\tau(E)}t + \varphi_0, k \right], \quad (\text{C6})$$

where  $\tau(E)$  is the inverse of the oscillation frequency given by Eq. (11). Note that the precession period is defined as a time  $\tilde{\tau}$ , which appears in the elliptic function as  $\text{sn}(4Kt/\tilde{\tau}, k)$ . In fact, in the circular limit of the elliptic function, i.e.,  $k \rightarrow 0$ ,  $\text{sn}(y, k) \rightarrow \sin(y) = \sin(2\pi t/\tilde{\tau})$  because  $\lim_{k \rightarrow 0} K(k) = \pi/2$ , and thus  $\tilde{\tau}$  can be regarded as an oscillation period. The solution of the LL equation in different systems can be found in, for example, Refs. [71,80].

Since  $E = -M \int d\mathbf{m} \cdot \mathbf{H}$ , the energy change is described by the equation

$$\begin{aligned} \frac{dE}{dt} &= -M\mathbf{H} \cdot \frac{d\mathbf{m}}{dt} = -\alpha\gamma M[\mathbf{H}^2 - (\mathbf{m} \cdot \mathbf{H})^2] \\ &\quad + \gamma MH_s[\mathbf{p} \cdot \mathbf{H} - (\mathbf{m} \cdot \mathbf{p})(\mathbf{m} \cdot \mathbf{H})], \end{aligned} \quad (\text{C7})$$

where we substitute the right-hand side of Eq. (1) to  $d\mathbf{m}/dt$  in Eq. (C7) and neglect higher-order terms of  $\alpha$ . We note that the evaluation of Eq. (C7) requires, strictly speaking, the exact solution of the LLG equation. The exact solution of the LLG equation deviates from the solution of the LL equation, Eqs. (C4), (C5) and (C6), due to the presence of the spin-transfer and damping torques, and it is hard to obtain analytically. In addition, even if such a solution is obtained, it will depend on the initial condition, which is usually uncontrollable. However, when the damping constant and the current are small, the deviation is also small and the magnetization precesses many times before the switching, as described in the main text. In this case, the energy change described by Eq. (C7) is slow and becomes approximately independent

of the initial condition. When the energy change is slow, this change is well described by Eq. (C7) averaged over the precession trajectory. Note that this precession trajectory is also approximated by the solution of the LL equation because, although the spin-transfer and damping torques cause deviation, the deviation is small, as mentioned. After averaging Eq. (C7) over the precession trajectory, we obtain Eq. (5) with Eqs. (6) and (7). The explicit forms of  $\mathcal{W}_\alpha$  and  $\mathcal{W}_s$  for a specific system can be obtained by substituting the solution of the LL equation into Eqs. (6) and (7). For example, Eqs. (8) and (9) are obtained by substituting Eqs. (C4), (C5), and (C6) into Eqs. (6) and (7), respectively.

#### APPENDIX D: DEFINITIONS OF $J_c$ AND $J^*$

Here, we discuss the definitions and derivation of Eqs. (16) and (17). For this purpose, let us briefly review the physical interpretation of Eq. (5).

The precession torque,  $-\gamma \mathbf{m} \times \mathbf{H}$ , induces a precession of the magnetization on a constant energy curve, where the energy density  $E$  relates to the effective magnetic field  $\mathbf{H}$  via  $E = -M \int d\mathbf{m} \cdot \mathbf{H}$ . Therefore, when the spin-transfer torque compensates the damping torque, magnetization dynamics is dominated by the precession, and it becomes reasonable to average the LLG equation over a constant energy curve. Under such circumstances, we obtain Eq. (5) from Eq. (1). As discussed in Sec. II C, the condition for the compensation depends on many factors, such as the directions of the easy axis and spin polarization. In the following, as in the case of the main text, we assume that the spin-transfer torque compensates for the damping torque and thus the magnetization dynamics is dominated by the precession, under which the magnetization dynamics is well described by Eq. (5).

We note that  $\mathcal{W}_s$  given by Eq. (7) is proportional to the current density  $J$  through  $H_s$ . It is convenient to introduce  $\mathcal{Q}_s$  as  $\mathcal{W}_s = \mathcal{Q}_s J$  and define  $J(E)$  as

$$J(E) = -\frac{\mathcal{W}_\alpha}{\mathcal{Q}_s}. \quad (\text{D1})$$

Note that  $J(E)$  is the current density to sustain the magnetization precession on a constant energy curve of  $E$ . Now let us discuss the derivations of  $J_c$  and  $J^*$ . In the absence of current, the magnetization stays near the minimum energy state. Therefore, the current density required to destabilize the stable state is given by

$$J_c = J(E_{\min}). \quad (\text{D2})$$

When the current density becomes slightly larger than  $J_c$ , the spin-transfer torque overcomes the damping torque acting on the magnetization near the stable state ( $E = E_{\min}$ ), and the magnetization will move to a higher-energy state. Note that  $\mathcal{W}_\alpha$  and  $\mathcal{W}_s$  ( $\propto \mathcal{Q}_s$ ) often become zero in the limit of  $E \rightarrow E_{\min}$ , as mentioned in Sec. II D. Therefore, it is necessary to expand  $\mathcal{W}_\alpha$  and  $\mathcal{Q}_s$  near  $E = E_{\min}$ . Then, we arrive at Eq. (15).

The threshold current density for the switching is defined as

$$J^* = \max[J(E)], \quad (\text{D3})$$

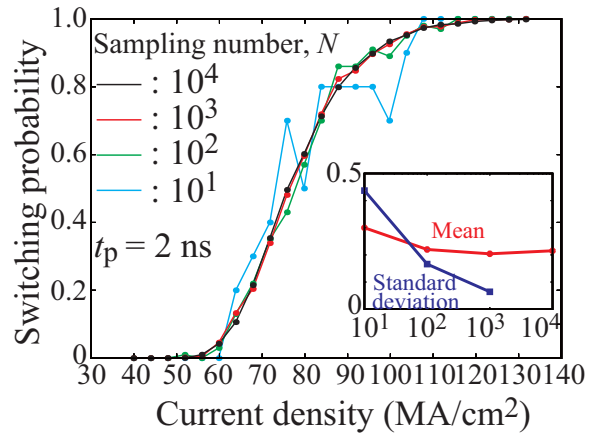


FIG. 9. The dependence of the switching probability on the number of trials in experiments. The inset shows the dependences of the mean and the standard deviation of the switching probability on the number of trials used in the evaluation, where the pulse width is 2 ns and the current density is 67.8 MA/cm<sup>2</sup>.

where the range of  $E$  is  $E_{\min} \leq E \leq E_d$ . The physical interpretation of Eq. (17) is as follows. Note that destabilization of the stable state, by applying a current density larger than  $J_c$ , does not guarantee switching. When the current density  $J$  is in the range of  $J/J_c > 1$  and  $J/J^* < 1$ , there are  $E$  satisfying  $\mathcal{W}_\alpha(E) + \mathcal{W}_s(E) = 0$ . When such an  $E$  exists, auto-oscillation of the magnetization is excited. On the other hand, when the current density is larger than  $J^*$ , there is no  $E$  satisfying  $\mathcal{W}_\alpha(E) + \mathcal{W}_s(E) = 0$ . Therefore, the magnetization cannot maintain the auto-oscillation state, and it switches its direction. Accordingly,  $J^*$  defined by Eq. (D3) can be regarded as the threshold current density for switching.

In the case of in-plane magnetized ferromagnets, where  $\mathcal{W}_\alpha$  and  $\mathcal{W}_s$  are given by Eqs. (8) and (9), respectively,  $J(E)$  given by Eq. (D1) monotonically increases with  $E$ . Therefore,  $J^*$  is given by  $J^* = J(E_d)$ , where the explicit form is given by Eq. (17). It is well known that in-plane magnetized ferromagnets can show auto-oscillation when the value of the current density is appropriately controlled [45]. On the other hand, for a perpendicularly magnetized system,  $J(E)$  is obtained from Eq. (25) as

$$J(\theta) = \frac{2\alpha e M d}{\hbar \vartheta} H_K \cos \theta, \quad (\text{D4})$$

where we use the tilt angle  $\theta$  instead of the energy density  $E = -(MH_K/2) \cos^2 \theta$ . Note that the minimum (saddle) energy state corresponds to  $\theta = 0$  ( $\pi/2$ ). Therefore, Eq. (D4) is a monotonic decreasing function of  $E$ . Accordingly,  $J^* = J(E_{\min}) = J_c$  in this system. Once the minimum energy state is destabilized by the spin-transfer torque, the magnetization always switches its direction, and auto-oscillation cannot be excited.

#### APPENDIX E: ACCURACY OF THE SWITCHING PROBABILITY IN EXPERIMENTS

Here, we discuss the accuracy of the switching probability obtained in the experiments. We divided the  $10^4$  measure-

ments into 10 subgroups, with each subgroup containing  $N$  measurement results. We vary  $N$  as 10, 100, 1000. The data for each subgroup are randomly selected. Figure 9 shows the dependence of the switching probability on the current density with various  $N$ . As an example, we chose data with the pulse width set to 2 ns. The black circles are identical to those shown in Fig. 7(a). As is evident, scattering of the data increases with decreasing  $N$ .

The inset to Fig. 9 shows the dependence of the mean value and standard deviation of the switching probability

for the 10 subgroups. Data with current density equal to  $67.8 \text{ MA/cm}^2$  are chosen as an example (pulse width is 2 ns). (For the mean value of the switching probability, we also included the results with  $N = 10^4$ . Since there is only one subgroup for  $N = 10^4$ , the standard deviation is not shown.) While the standard deviation continues to reduce with increasing  $N$ , the mean value tends to saturate as  $N$  is increased. These results show that the  $10^4$  trial is sufficient to study the current dependence of the switching probability.

- [1] J. C. Slonczewski, Current-driven excitation of magnetic multilayers, *J. Magn. Magn. Mater.* **159**, L1 (1996).
- [2] L. Berger, Emission of spin waves by a magnetic multilayer traversed by a current, *Phys. Rev. B* **54**, 9353 (1996).
- [3] J. C. Slonczewski, Currents, torques, and polarization factors in magnetic tunnel junctions, *Phys. Rev. B* **71**, 024411 (2005).
- [4] J. A. Katine, F. J. Albert, R. A. Buhrman, E. B. Myers, and D. C. Ralph, Current-Driven Magnetization Reversal and Spin-Wave Excitations in Co/Cu/Co Pillars, *Phys. Rev. Lett.* **84**, 3149 (2000).
- [5] E. B. Myers, F. J. Albert, J. C. Sankey, E. Bonet, R. A. Buhrman, and D. C. Ralph, Thermally Activated Magnetic Reversal Induced by a Spin-Polarized Current, *Phys. Rev. Lett.* **89**, 196801 (2002).
- [6] S. I. Kiselev, J. C. Sankey, I. N. Krivorotov, N. C. Emley, R. J. Schoelkopf, R. A. Buhrman, and D. C. Ralph, Microwave oscillations of a nanomagnet driven by a spin-polarized current, *Nature (London)* **425**, 380 (2003).
- [7] H. Kubota, A. Fukushima, Y. Ootani, S. Yuasa, K. Ando, H. Maehara, K. Tsunekawa, D. D. Djayaprawira, N. Watanabe, and Y. Suzuki, Evaluation of spin-transfer switching in CoFeB/MgO/CoFeB magnetic tunnel junctions, *Jpn. J. Appl. Phys.* **44**, L1237 (2005).
- [8] I. N. Krivorotov, N. C. Emley, J. C. Sankey, S. I. Kiselev, D. C. Ralph, and R. A. Buhrman, Time-domain measurements of nanomagnet dynamics driven by spin-transfer torques, *Science* **307**, 228 (2005).
- [9] P. M. Braganca, I. N. Krivorotov, O. Ozatay, A. G. F. Garcia, N. C. Emley, J. C. Sankey, D. C. Ralph, and R. A. Buhrman, Reducing the critical current for short-pulse spin-transfer switching of nanomagnets, *Appl. Phys. Lett.* **87**, 112507 (2005).
- [10] Z. Diao, D. Apalkov, M. Pakala, Y. Ding, A. Panchula, and Y. Huai, Spin transfer switching and spin polarization in magnetic tunnel junctions with MgO and  $\text{AlO}_x$  barriers, *Appl. Phys. Lett.* **87**, 232502 (2005).
- [11] S. Parkin, X. Jiang, C. Kaiser, A. Panchula, K. Roche, and M. Samant, Magnetically engineered spintronic sensors and memory, *Proc. IEEE* **91**, 661 (2003).
- [12] *Spin Dynamics in Confined Magnetic Structures III*, edited by B. Hillebrands and A. Thiaville (Springer, Berlin, 2006).
- [13] L. Thomas, G. Jan, J. Zhu, H. Liu, Y.-J. Lee, S. Le, R.-Y. Tong, K. Pi, Y.-J. Wang, D. Shen, R. He, J. Haq, J. Teng, V. Lam, K. Huang, T. Zhong, T. Torng, and P.-K. Wang, Perpendicular spin transfer torque magnetic random access memories with high spin torque efficiency and thermal stability for embedded applications, *J. Appl. Phys.* **115**, 172615 (2014).
- [14] *Introduction to Magnetic Random-Access Memory*, edited by B. Dieny, R. B. Goldfarb, and K.-J. Lee (Wiley-IEEE, Hoboken, NJ, 2016).
- [15] K. Garello, F. Yasin, S. Couet, L. Souriau, J. Swerts, S. Rao, S. V. Beek, W. Kim, E. Liu, S. Kundu, D. Tsvetanova, K. Croes, N. Jossart, E. Grimaldi, M. Baumgartner, D. Crotti, A. Fumémont, P. Gambardella, and G. S. Kar, SOT-MRAM 300 MM Integration for Low Power and Ultrafast Embedded Memories, *2018 IEEE Symposium on VLSI Circuits (IEEE, Piscataway, NJ, 2018)*, p. 81.
- [16] M. Cubukcu, O. Boule, N. Mikuszeit, C. Hamelin, T. Brächer, N. Lamard, M.-C. Cyrille, L. Buda-Prejbeanu, K. Garello, I. M. Miron, O. Klein, G. de Loubens, V. V. Naletov, J. Langer, B. Ocker, P. Gambardella, and G. Gaudin, Ultra-fast perpendicular spin-orbit torque MRAM, *IEEE Trans. Magn.* **54**, 9300204 (2018).
- [17] J.-G. Zhu and Y. Wang, Microwave assisted magnetic recording utilizing perpendicular spin torque oscillator with switchable perpendicular electrodes, *IEEE Trans. Magn.* **46**, 751 (2010).
- [18] A. Fukushima, T. Seki, K. Yakushiji, H. Kubota, H. Imamura, S. Yuasa, and K. Ando, Spin dice: A scalable truly random number generator based on spintronics, *Appl. Phys. Express* **7**, 083001 (2014).
- [19] W. F. Brown Jr., Thermal fluctuations of a single-domain particle, *Phys. Rev.* **130**, 1677 (1963).
- [20] R. H. Koch, J. A. Katine, and J. Z. Sun, Time-Resolved Reversal of Spin-Transfer Switching in a Nanomagnet, *Phys. Rev. Lett.* **92**, 088302 (2004).
- [21] T. Aoki, Y. Ando, D. Watanabe, M. Oogane, and T. Miyazaki, Spin transfer switching in the nanosecond regime for CoFeB/MgO/CoFeB ferromagnetic tunnel junctions, *Appl. Phys. Lett.* **103**, 103911 (2008).
- [22] J. Hayakawa, S. Ikeda, K. Miura, M. Yamanouchi, Y. M. Lee, R. Sasaki, M. Ichimura, K. Ito, T. Kawahara, R. Takemura, T. Meguro, F. Matsukura, H. Takahashi, H. Matsuoka, and H. Ohno, Current-induced magnetization switching in mgo barrier magnetic tunnel junctions with CoFeB-based synthetic ferrimagnetic free layers, *IEEE Trans. Magn.* **44**, 1962 (2008).
- [23] S. Yakata, H. Kubota, T. Sugano, T. Seki, K. Yakushiji, A. Fukushima, S. Yuasa, and K. Ando, Thermal stability and spin-transfer switchings in MgO-based magnetic tunnel junctions with ferromagnetically and antiferromagnetically coupled synthetic free layers, *Appl. Phys. Lett.* **95**, 242504 (2009).

- [24] Y. Suzuki, A. A. Tulapurkar, and C. Chappert, *Nanomagnetism and Spintronics*, edited by T. Shinjo (Elsevier, Amsterdam, 2009), Chap. 3.
- [25] H. Tomita, T. Nozaki, T. Seki, T. Nagase, K. Nishiyama, E. Kitagawa, M. Yoshikawa, T. Daibou, M. Nagamine, T. Kishi, S. Ikegawa, N. Shimomura, H. Yoda, and Y. Suzuki, High-speed spin-transfer switching in GMR nano-pillars with perpendicular anisotropy, *IEEE Trans. Magn.* **47**, 1599 (2011).
- [26] H. Sato, M. Yamanouchi, K. Miura, S. Ikeda, H. D. Gan, K. Mizunuma, R. Koizumi, F. Matsukura, and H. Ohno, Junction size effect on switching current and thermal stability in CoFeB/MgO perpendicular magnetic tunnel junctions, *Appl. Phys. Lett.* **99**, 042501 (2011).
- [27] H. Tomita, S. Miwa, T. Nozaki, S. Yamashita, T. Nagase, K. Nishiyama, E. Kitagawa, M. Yoshikawa, T. Daibou, M. Nagamine, T. Kishi, S. Ikegawa, N. Shimomura, H. Yoda, and Y. Suzuki, Unified understanding of both thermally assisted and precessional spin-transfer switching in perpendicularly magnetized giant magnetoresistive nanopillars, *Appl. Phys. Lett.* **102**, 042409 (2013).
- [28] M. Yamanouchi, L. Chen, J. Kim, M. Hayashi, H. Sato, S. Fukami, S. Ikeda, F. Matsukura, and H. Ohno, Three terminal magnetic tunnel junction utilizing the spin Hall effect of iridium-doped copper, *Appl. Phys. Lett.* **102**, 212408 (2013).
- [29] K. Yakushiji, A. Fukushima, H. Kubota, M. Konoto, and S. Yuasa, Ultralow-voltage spin-transfer switching in perpendicularly magnetized magnetic tunnel junctions with synthetic antiferromagnetic reference layer, *Appl. Phys. Express* **6**, 113006 (2013).
- [30] D. B. Gopman, D. Bedau, S. Mangin, E. E. Fullerton, J. A. Katine, and A. D. Kent, Switching field distribution with spin transfer torques in perpendicularly magnetized spin-valve nanopillars, *Phys. Rev. B* **89**, 134427 (2014).
- [31] L. Liu, C.-F. Pai, Y. Li, H. W. Tseng, D. C. Ralph, and R. A. Buhrman, Spin-torque switching with the giant spin hall effect of tantalum, *Science* **336**, 555 (2012).
- [32] C.-F. Pai, L. Liu, Y. Li, H. W. Tseng, D. C. Ralph, and R. A. Buhrman, Spin transfer torque devices utilizing the giant spin Hall effect of tungsten, *Appl. Phys. Lett.* **101**, 122404 (2012).
- [33] Y. Shiokawa, E. Komura, Y. Ishitani, A. Tsumita, K. Suda, Y. Kakinuma, and T. Sasaki, High write endurance up to  $10^{12}$  cycles in a spin current-type magnetic memory array, *AIP Adv.* **9**, 035236 (2019).
- [34] Y. Shiokawa, E. Komura, Y. Ishitani, A. Tsumita, K. Suda, K. Hamanaka, T. Taniguchi, and T. Sasaki, Dependency of high-speed write properties on external magnetic field in spin-orbit torque in-plane magnetoresistance devices, *Appl. Phys. Express* **14**, 013001 (2021).
- [35] S. Isogami, Y. Shiokawa, A. Tsumita, E. Komura, Y. Ishitani, K. Hamanaka, T. Taniguchi, S. Mitani, T. Sasaki, and M. Hayashi, Spin-orbit torque driven magnetization switching in W/CoFeB/MgO-based type-Y three terminal magnetic tunnel junctions, *Sci. Rep.* **11**, 16676 (2021).
- [36] J. Z. Sun, Spin-current interaction with a monodomain magnetic body: A model study, *Phys. Rev. B* **62**, 570 (2000).
- [37] J. He, J. Z. Sun, and S. Zhang, Switching speed distribution of spin-torque-induced magnetic reversal, *J. Appl. Phys.* **101**, 09A501 (2007).
- [38] D. Bedau, H. Liu, J. Z. Sun, J. A. Katine, E. E. Fullerton, S. Mangin, and A. D. Kent, Spin-transfer pulse switching: From the dynamic to the thermally activated regime, *Appl. Phys. Lett.* **97**, 262502 (2010).
- [39] D. M. Apalkov and P. B. Visscher, Spin-torque switching: Fokker-Planck rate calculation, *Phys. Rev. B* **72**, 180405(R) (2005).
- [40] T. Taniguchi and H. Imamura, Thermally assisted spin transfer torque switching in synthetic free layers, *Phys. Rev. B* **83**, 054432 (2011).
- [41] W. H. Butler, T. Mewes, C. K. A. Mewes, P. B. Visscher, W. H. Rippard, S. E. Russek, and R. Heindl, Switching distribution for perpendicular spin-torque devices within the macrospin approximation, *IEEE Trans. Magn.* **48**, 4684 (2012).
- [42] T. Taniguchi and H. Imamura, Thermal switching rate of a ferromagnetic material with uniaxial anisotropy, *Phys. Rev. B* **85**, 184403 (2012).
- [43] T. Taniguchi, M. Shibata, M. Marthaler, Y. Utsumi, and H. Imamura, Numerical study on spin torque switching in thermally activated region, *Appl. Phys. Express* **5**, 063009 (2012).
- [44] K. A. Newhall and E. Vanden-Eijnden, Averaged equation for energy diffusion on a graph reveals bifurcation diagram and thermally assisted reversal times in spin-torque driven nanomagnets, *J. Appl. Phys.* **113**, 184105 (2013).
- [45] T. Taniguchi, Y. Utsumi, M. Marthaler, D. S. Golubev, and H. Imamura, Spin torque switching of an in-plane magnetized system in a thermally activated region, *Phys. Rev. B* **87**, 054406 (2013).
- [46] D. Li, A. Smogunov, C. Barreteau, F. Ducastelle, and D. Spanjaard, Thermally activated switching rate of a nanomagnet in the presence of spin torque, *Phys. Rev. B* **88**, 214413 (2013).
- [47] D. Pinna, A. D. Kent, and D. L. Stein, Thermally-assisted spin-transfer torque magnetization reversal of uniaxial nanomagnets in energy space, *IEEE Trans. Magn.* **49**, 3144 (2013).
- [48] J. Z. Sun, R. P. Robertazzi, J. Nowak, P. L. Trouilloud, G. Hu, D. W. Abraham, M. C. Gaidis, S. L. Brown, E. J. O'Sullivan, W. J. Gallagher, and D. C. Worledge, Effect of subvolume excitation and spin-torque efficiency on magnetic switching, *Phys. Rev. B* **84**, 064413 (2011).
- [49] J. Z. Sun, S. L. Brown, W. Chen, E. A. Delenia, M. C. Gaidis, J. Harms, G. Hu, X. Jiang, R. Kilaru, W. Kula, G. Lauer, L. Q. Liu, S. Murthy, J. Nowak, E. J. O'Sullivan, S. S. P. Parkin, R. P. Robertazzi, P. M. Rice, G. Sandhu, T. Topuria *et al.*, Spin-torque switching efficiency in CoFeB-MgO based tunnel junctions, *Phys. Rev. B* **88**, 104426 (2013).
- [50] G. D. Chaves-O'Flynn, G. Wolf, J. Z. Sun, and A. D. Kent, Thermal Stability of Magnetic States in Circular Thin-Film Nanomagnets with Large Perpendicular Magnetic Anisotropy, *Phys. Rev. Appl.* **4**, 024010 (2015).
- [51] J. Z. Sun, Spin-transfer torque switching probability of CoFeB/MgO/CoFeB magnetic tunnel junctions beyond macrospin, *Phys. Rev. B* **104**, 104428 (2021).
- [52] L. Liu, O. J. Lee, T. J. Gudmundsen, D. C. Ralph, and R. A. Buhrman, Current-Induced Switching of Perpendicularly Magnetized Magnetic Layers Using Spin Torque from the Spin Hall Effect, *Phys. Rev. Lett.* **109**, 096602 (2012).
- [53] G. Yu, P. Upadhyaya, Y. Fan, J. G. Alzate, W. Jiang, K. L. Wong, S. Takei, S. A. Bender, L.-T. Chang, Y. Jiang, M. Lang, J. Tang, Y. Wang, Y. Tserkovnyak, P. K. Amiri, and K. L. Wang, Switching of a perpendicular magnetization by spin-orbit torques in

- the absence of external magnetic fields, *Nat. Nanotechnol.* **9**, 548 (2014).
- [54] M. Cubukcu, O. Bouille, M. Drouard, K. Garello, C. O. Avci, I. M. Miron, J. Langer, B. Ocker, P. Gambardella, and G. Gaudin, Spin-orbit torque magnetization switching of a three-terminal perpendicular magnetic tunnel junction, *Appl. Phys. Lett.* **104**, 042406 (2014).
- [55] L. You, O. L. D. Bhowmik, D. Labanowski, J. Hong, J. Bokor, and S. Salahuddin, Switching of perpendicularly polarized nanomagnets with spin orbit torque without an external magnetic field by engineering a tilted anisotropy, *Proc. Natl. Acad. Sci. (USA)* **112**, 10310 (2015).
- [56] J. Torrejon, F. Garcia-Sanchez, T. Taniguchi, J. Sinha, S. Mitani, J.-V. Kim, and M. Hayashi, Current-driven asymmetric magnetization switching in perpendicularly magnetized CoFeB/MgO heterostructures, *Phys. Rev. B* **91**, 214434 (2015).
- [57] Y.-C. Lau, D. Betto, K. Rode, J. M. D. Coey, and P. Stamenov, Spin-orbit torque switching without an external field using interlayer exchange coupling, *Nat. Nanotechnol.* **11**, 758 (2016).
- [58] A. van den Brink, G. Vermijs, A. Solignac, J. Koo, J. T. Kohlhepp, H. J. M. Swagten, and B. Koopmans, Field-free magnetization reversal by spin-Hall effect and exchange bias, *Nat. Commun.* **7**, 10854 (2016).
- [59] Y.-W. Oh, S. H. C. Baek, Y. M. Kim, H. Y. Lee, K.-D. Lee, C.-G. Yang, E.-S. Park, K.-S. Lee, K.-W. Kim, G. Go, J.-R. Jeong, B.-C. Min, H.-W. Lee, K.-J. Lee, and B.-G. Park, Field-free switching of perpendicular magnetization through spin-orbit torque in antiferromagnet/ferromagnet/oxide structures, *Nat. Nanotechnol.* **11**, 878 (2016).
- [60] S. Fukami, T. Anekawa, C. Zhang, and H. Ohno, Magnetization switching by spin-orbit torque in an antiferromagnet-ferromagnet bilayer system, *Nat. Mater.* **15**, 535 (2016).
- [61] K. Garello, I. M. Miron, C. O. Avci, F. Freimuth, Y. Mokrousov, S. Blügel, S. Auffret, O. Bouille, G. Gaudin, and P. Gambardella, Symmetry and magnitude of spin-orbit torques in ferromagnetic heterostructures, *Nat. Nanotechnol.* **8**, 587 (2013).
- [62] A. Manchon, J. Železný, I. M. Miron, T. Jungwirth, J. Sinova, A. Thiaville, K. Garello, and P. Gambardella, Current-induced spin-orbit torques in ferromagnetic and antiferromagnetic systems, *Rev. Mod. Phys.* **91**, 035004 (2019).
- [63] M. Beleggia, M. D. Graef, Y. T. Millev, D. A. Goode, and G. Rowlands, Demagnetization factors for elliptic cylinders, *J. Phys. D* **38**, 3333 (2005).
- [64] J. Grollier, V. Cros, H. Jaffrés, A. Hamzic, J. M. George, G. Faini, J. B. Youssef, H. LeGall, and A. Fert, Field dependence of magnetization reversal by spin transfer, *Phys. Rev. B* **67**, 174402 (2003).
- [65] T. Taniguchi, S. Mitani, and M. Hayashi, Critical current destabilizing perpendicular magnetization by the spin Hall effect, *Phys. Rev. B* **92**, 024428 (2015).
- [66] K.-S. Lee, S.-W. Lee, B.-C. Min, and K.-J. Lee, Theoretical current for switching of a perpendicular magnetic layer induced by spin Hall effect, *Appl. Phys. Lett.* **102**, 112410 (2013).
- [67] K.-S. Lee, S.-W. Lee, B.-C. Min, and K.-J. Lee, Thermally activated switching of perpendicular magnet by spin-orbit spin torque, *Appl. Phys. Lett.* **104**, 072413 (2014).
- [68] T. Taniguchi, Theoretical condition for switching the magnetization in a perpendicularly magnetized ferromagnet via the spin Hall effect, *Phys. Rev. B* **100**, 174419 (2019).
- [69] T. Taniguchi, Switching induced by spin Hall effect in an in-plane magnetized ferromagnet with the easy axis parallel to the current, *Phys. Rev. B* **102**, 104435 (2020).
- [70] D.-K. Lee and K.-J. Lee, Spin-orbit torque switching of perpendicular magnetization in ferromagnetic trilayers, *Sci. Rep.* **10**, 1772 (2020).
- [71] G. Bertotti, I. Mayergoyz, and C. Serpico, *Nonlinear Magnetization Dynamics in Nanosystems* (Elsevier, Amsterdam, 2009).
- [72] T. Taniguchi, H. Arai, S. Tsunegi, S. Tamaru, H. Kubota, and H. Imamura, Critical field of spin torque oscillator with perpendicularly magnetized free layer, *Appl. Phys. Express* **6**, 123003 (2013).
- [73] S. Fukami, T. Anekawa, C. Zhang, and H. Ohno, A spin-orbit torque switching scheme with collinear magnetic easy axis and current configuration, *Nat. Nanotechnol.* **11**, 621 (2016).
- [74] Q. Shao, P. Li, L. Liu, H. Yang, S. Fukami, A. Razavi, H. Wu, K. Wang, F. Freimuth, Y. Mokrousov, M. D. Stiles, S. Emori, A. Hoffmann, J. Åkerman, K. Roy, J.-P. Wang, and S.-H. Yang, Roadmap of Spin-Orbit torques, *IEEE Trans. Magn.* **57**, 800439 (2021).
- [75] T. Taniguchi, Dynamic coupling of ferromagnets via spin Hall magnetoresistance, *Phys. Rev. B* **95**, 104426 (2017).
- [76] T. Taniguchi and H. Imamura, Maximizing spin torque diode voltage by optimizing magnetization alignment, *Appl. Phys. Express* **6**, 053002 (2013).
- [77] X. Wang, W. Zhu, M. Siegert, and D. Dimitrov, Spin torque induced magnetization switching variations, *IEEE Trans. Magn.* **45**, 2038 (2009).
- [78] A. F. Vincent, N. Locatelli, J.-O. Klein, W. S. Zhao, S. Galdin-Retailleau, and D. Querlioz, Analytical macrospin modeling of the stochastic switching time of spin-transfer torque device, *IEEE Trans. Electron Devices* **62**, 164 (2015).
- [79] H. Risken, *The Fokker-Planck Equation*, 2nd ed. (Springer, Berlin, 1989), Chap. 3.
- [80] Y. Kurokawa, K. Yamada, T. Taniguchi, S. Horiike, T. Tanaka, and H. Yuasa, Ultra-wide-band millimeter-wave generator using spin torque oscillator with strong interlayer exchange couplings, *Sci. Rep.* **12**, 10849 (2022).